Evolution of depositional settings in the Torrey area during the Smithian (Early Triassic, Utah, USA) and their significance for the biotic recovery.

Nicolas Olivier, Arnaud Brayard, Emmanuelle Vennin, Gilles Escarguel, Emmanuel Fara, Kevin G. Bylund, James F. Jenks, Gwénaël Caravaca, Daniel A. Stephen

This article has been accepted in January, 2015 for publication in Geological Journal©, p*ublished by Wiley. All rights reserved.*

DOI: 10.1002/gj.2663

(http://onlinelibrary.wiley.com/doi/10.1002/gj.2663/abstract)

Evolution of depositional settings in the Torrey area during the Smithian (Early Triassic, Utah, USA) and their significance for the biotic recovery

NICOLAS OLIVIER[1*], ARNAUD BRAYARD[2], EMMANUELLE VENNIN[2], GILLES ESCARGUEL[3], EMMANUEL FARA[2], KEVIN G. BYLUND[4], JAMES F. JENKS[5], GWÉNAËL CARAVACA[2] and DANIEL A. STEPHEN[6]

[1]*Laboratoire Magmas et Volcans, Université Blaise Pascal – CNRS – IRD, OPGC, 5 rue Kessler, 63038 Clermont-Ferrand, France*

[2]*UMR CNRS 6282 Biogéosciences, Université de Bourgogne, 6 boulevard Gabriel, 21000 Dijon, France*

[3]*Laboratoire de Géologie de Lyon : Terre, Planètes, Environnement, UMR CNRS 5276, Université Lyon 1, 69622 Villeurbanne cedex, France*

[4]*Kevin G. Bylund, 140 South 700 East, Spanish Fork, Utah 84660, USA*

[5]*James F. Jenks, 1134 Johnson Ridge Lane, West Jordan, Utah 84084, USA*

[6]*Daniel A. Stephen, Department of Earth Science, Utah Valley University, 800 West University Parkway, Orem, Utah 84058, USA*

**Correspondence to: N. Olivier, Laboratoire Magmas et Volcans, Université Blaise Pascal – CNRS – IRD, OPGC, 5 rue Kessler, 63038 Clermont-Ferrand, France. E-mail: n.olivier@opgc.fr*

ABSTRACT

This work focuses on well-exposed Lower Triassic sedimentary rocks in the area of Torrey (south-central Utah, USA). The studied Smithian deposits record a large-scale 3rd order sea-level cycle, which permits a detailed reconstruction of the evolution of depositional settings. During the middle Smithian, peritidal microbial limestones associated with a rather low-

diversity benthic fauna were deposited seaward of the tidal flat siliciclastic red beds. Associated with siliceous sponges, microbial limestones formed small m-scale patch reefs. During the late middle to late Smithian interval, the sedimentary system is characterized by tidal flat dolostones of an interior platform, ooid-bioclastic deposits of a tide-dominated shoal complex, and mid-shelf bioclastic limestones. Microbial deposits, corresponding to sparse stromatolites formed in the interior platform, are contemporaneous with a well-diversified marine fauna living in a seaward shoal complex and mid-shelf area. The nature and distribution of these Smithian microbial deposits are not related to any particular deleterious environmental condition, highlighting that observed patterns of biotic recovery after the end-Permian mass extinction were directly influenced by depositional settings. Facies evolution and stratal stacking patterns allow us to identify large, medium and small-scale, as well as elementary depositional sequences. Large and medium-scale sequences are consistent with sea-level changes, whereas small-scale and elementary sequences are better explained by autocyclic processes.

KEYWORDS: Early Triassic; Smithian; Utah; microbialites; depositional environments; biotic recovery; bioconstructions

---

1. INTRODUCTION

Deleterious oceanic conditions are generally associated with the aftermath of the Permian-Triassic mass extinction, the most devastating biotic crisis in the Phanerozoic (Raup, 1979, Erwin, 2006). Indeed, large environmental perturbations, combining ocean acidification, anoxia, euxinia, and fluctuating productivity (Payne *et al.*, 2004; Galfetti *et al.*, 2007; Grasby *et al.*, 2013), likely constrained the biotic recovery during the Early Triassic. Until recently, post-crisis environments appeared to be particularly suitable for widespread development of abiotic and microbial deposits (Schubert and Bottjer, 1992; Baud *et al.*, 1997, 2007; Mata and Bottjer, 2012; Woods, 2013), whereas the metazoan recovery was assumed to be delayed. However, for some marine groups such as ammonoids (Brayard *et al.*, 2009b) and conodonts (Orchard, 2007), or where permitted by favorable environmental conditions (Krystyn *et al.*,

2003; Twitchett *et al.*, 2004; Chen *et al.*, 2007; Beatty *et al.*, 2008; Zonneveld *et al.*, 2010; Brayard *et al.*, 2011; Hautmann *et al.*, 2011, 2013; Kaim *et al.*, 2010; Hofmann *et al.*, 2011, 2013a, b), life seems to have recovered rapidly in the Early Triassic. The timing and modalities of the biotic recovery are therefore still debated, highlighting the importance of its spatio-temporal variations, especially from the point of view of the underlying depositional settings (Pruss *et al.*, 2006; Beatty *et al.*, 2008; Galfetti *et al.*, 2008; Brühwiler *et al.*, 2009; Mata and Bottjer, 2011, 2012; Kershaw *et al.*, 2012; Sano *et al.*, 2012; Komatsu *et al.*, 2014; Pietsch and Bottjer, 2014; Olivier *et al.*, 2014). Therefore, detailed sedimentological studies and palaeoenvironmental reconstructions are of primary importance for improving our knowledge of the Early Triassic biotic recovery.

In the Torrey area (south central Utah, USA), excellent, widespread exposures of Lower Triassic deposits occur within and near Capitol Reef National Park (Fig. 1). In this area, the lithological succession includes Permian limestones, red beds of the Black Dragon Formation, microbial and bioclastic limestones of the Smithian Sinbad Formation, and sediments up to and including the red beds of the Spathian Torrey Formation (Stewart *et al.*, 1972, Blakey, 1974, 1977; Dean, 1981). The variety of deposits and number of potential sections represent a good opportunity for detailed three-dimensional analysis of rapid lateral and vertical facies changes (Dean, 1981). However, the only previous attempt at section correlation in the Torrey area was largely based on a lithostratigraphic approach (Dean, 1981). This work presents a detailed bed-by-bed sedimentological analysis of three sections in the area southeast of Torrey (Fig. 1a). Its main objectives include: (i) analyse the nature and diversity of facies in order to obtain robust depositional environmental reconstructions; (ii) achieve sequential analysis of these sections in order to obtain highly-resolved correlation and discuss the effect of relative sea-level fluctuations on sedimentation with regard to autocyclic and allocyclic processes; and (iii) discuss the evolution of local depositional settings and its potential influence on biotic recovery at the regional level.

2. GEOLOGICAL SETTING

The three studied outcrops are located near the town of Torrey (Wayne County, southern Utah, USA; Fig. 1a) as follows: (i) French Fork section (38°15'32.11"N, 111°24'36.31"W), situated 4 km south of Torrey; (ii) Beas Lewis Flats section (38°17'0.98"N, 111°18'49.07"W), located about 6 km west of the small town of Fruita; and (iii) Pleasant Creek section

(38°10'21.58"N, 111°11'54.89"W), situated within Capitol Reef National Park, 13 km south of Fruita.

In the Torrey area, the Lower Triassic sedimentary succession is represented by interfingered siliciclastic and carbonate deposits (Blakey, 1974; Dean, 1981; Goodspeed and Lucas, 2007). These sediments belong to the Moenkopi and Thaynes groups (*sensu* Lucas *et al.*, 2007), which unconformably overly the Permian carbonate Kaibab Formation (Blakey, 1974; Dean, 1981). Directly above the Permian rocks, the Black Dragon Formation corresponds to the first occurrence of red beds (Fig. 1b). These siliciclastic deposits correspond to reddish to brownish siltstones, sandstones and even conglomerates (Blakey, 1974; Dean, 1981). The transition to the carbonate deposits of the Smithian Sinbad Formation can be gradual. Although, Dean (1981) placed the boundary between the Black Dragon and the Sinbad formations below the first carbonate bed, other workers considered transitional carbonate beds observed within the red beds as part of the Black Dragon Formation (Blakey, 1974; Goodspeed and Lucas, 2007). This work follows the lithostratigraphical definition of Dean (1981). The Sinbad Formation can be readily subdivided into two main units (Fig. 1b): a massive microbial limestone unit (lower Sinbad Formation) and a bioclastic limestone unit (upper Sinbad Formation). Contact with the overlying deposits of the Spathian Torrey Formation is classically described as a conformable surface between the bioclastic limestones of the Sinbad Formation and a second occurrence of red beds (Blakey, 1974; Dean, 1981).

During the Early Triassic, the western USA basin was located at a near-equatorial position on the western margin of the Pangea. A large epicontinental sea about 500 to 600 km-wide and extending from southern Utah to British Columbia, exhibited a deepening trend from the south-east to the north-west (Blakey, 1974; Paull and Paull, 1993; Goodspeed and Lucas, 2007). Thus, most of the terrigenous sediments belonging to the Moenkopi Group can be found in southern and southeastern Utah and they represent the most proximal settings and paleoshoreline positions (Olivier *et al.*, 2014). Carbonate deposits of the Thaynes Group represent more open-marine conditions and can be found mainly in central and northwestern Utah, southeastern Idaho and northeastern Nevada (Kummel, 1954; Hose and Repenning, 1959; Blakey, 1974; Collinson and Hasenmueller, 1978; Dean, 1981; Goodspeed and Lucas, 2007; Guex *et al.*, 2010; Brayard *et al.*, 2011, 2013).

Preliminary information regarding regional ammonoid and conodont biostratigraphy, from previous studies indicate that the Sinbad Formation in the Torrey area is late Smithian (*sensu* Brühwiler *et al.*, 2010) in age due to the occurrence of the *Anasibirites kingianus* zone (Stewart *et al.*, 1972; Blakey, 1974; Dean, 1981, Lucas *et al.*, 2007; Goodspeed and Lucas,

2007). Several new ammonoid specimens,collected bed-by-bed from the Torrey area, have been integrated with the new regional biostratigraphic framework proposed by Brayard *et al.* (2013). *Juvenites* aff. *spathi*, *Parussuria compressa*, *Meekoceras gracilitatis* and *Lanceolites compactus* occur in the uppermost part of the lower Sinbad Formation (interval A1; Fig. 1b), suggesting a likely middle Smithian age (basal *Owenites* beds by comparison with neighbouring localities; see Brayard *et al.*, 2013). Interval A2, situated in the middle of the upper Sinbad Formation, yields ammonoids identified as *Lanceolites compactus*, *Hedenstroemia kossmati*, *Churkites noblei*, *Guodunites hooveri* and *Dienoceras dieneri*. Such an assemblage is diagnostic of the *Owenites* beds, which are typically middle Smithian in age (Brayard *et al.*, 2009a, 2013). Interval A3 includes *Wasatchites perrini* and *Anasibirites kingianus*, indicating a late Smithian age (Brayard *et al.*, 2013). Rare conodonts occurring near the base of the upper Sinbad Formation are represented by *Furnishius triserratus*, *Parachirognathus ethingtoni* and some ellisonids, also indicating a Smithian age (N. Goudemand, pers. com. 2012).

3. SECTIONS AND FACIES DESCRIPTION

3.1. French Fork section

The Permian Kaibab limestones are not exposed at the base of the French Fork section (Fig. 2a). The entire section can be subdivided into three main lithological units (Figs 3, 4). The first unit includes the uppermost 12 m of red beds of the Black Dragon Formation (Fig. 1b). Facies (F1) consists of mm- to cm-thick red, dolosiltstone beds with small asymmetrical ripples (Table 1). Some muddy sheets display mud cracks locally. Other observed sedimentary structures include megaripples and climbing ripples. Quartz grains are abundant and subangular to subrounded. Also present are few cm- to dm-thick beds particularly rich in secondary gypsum.

The second unit occupying the interval between 12 and 23 m consists of two main limestone facies, which constitute the lower Sinbad Formation. Facies F2, which occurs only as a thin cm-thick interval at the base of this second lithological unit, corresponds to an intraclastic floatstone, with frequent basal erosive surfaces. Flat pebbles made of peloidal wackestone (locally mudstone or packstone) and exhibiting desiccation cracks are also present. Smaller intraclasts are poorly sorted and subangular to subrounded. A few domal stromatolites are visible locally.

Facies F3 corresponds to a massive peritidal limestone interval (Fig. 2a). Several undulating surfaces can be followed laterally along the cliff, permitting the identification of six meter-scale subunits (Fig. 4). These subunits consist of cm- to dm-thick beds that show important lateral variations in thickness. These variations tend to form local meter-scale patches (Figs 2a, 5a and b). In greater detail, two main subfacies can be identified at French Fork (Fig. 5c and d). The first fenestral limestone subfacies (F3b) is made of fenestrae, oncoids, peloids, aggregate grains, and some ooids and cortoids. Locally, some undulating laminated crusts binding the different grains are present (Fig. 5e and f). The sizes of the fenestrae are classically mm-scale, but some can be coalescent and form dm-scale aligned structures (Fig. 6a and d). Within these large fenestrae, microbialitic crusts are observed on the walls and roofs of the cavities with upward and downward growth direction (Fig. 6b and c, e). The relatively poor fauna is composed only of gastropods, bivalves, ostracods and siliceous sponges (Fig. 6f). Some fenestrae exhibit vadose silts (Fig. 7c). The second subfacies (F3c) consists of laminated micrites with domal and horizontal sheet cracks, and tepee structures (Figs 5g and h, 7d). Some stromatolites are also observed locally. The biota is sparse, consisting mainly of ostracods, gastropods, and siliceous sponges (Fig. 6g). Subfacies F3b an F3c can either be observed juxtaposed or superimposed (Fig. 7).

The third lithological unit, observed from 23 to 45 m, represents the upper Sinbad Formation. At French Fork, seven facies are identified in this uppermost lithological unit (Facies F5 and F8-F13; Fig. 4; Table 1). Facies F5 corresponds to dm- to m-thick intervals of dolostones with common cm-thick intercalations of siltstones and rare sandstones. Peloids and common-to-abundant subrounded quartz grains mainly represent non-biotic grains. This facies generally appears barren of organisms, but some ostracods and bivalve moldic voids can be observed. Evidence of infaunal activity is uncommon; only rare and localized trace fossils can be observed. Sedimentary structures are common and correspond to low-angle cross laminations. Facies F8 consists of ooid-bioclastic grainstone, which is only observed in a thin interval between 27 and 27.5 m. Facies F9 corresponds to peloid-bioclastic grainstone, which is also only observed within a thin interval at the top of the section (close to 45 m). Facies F10 is more frequent within the section, consisting of a grainstone (locally packstone) made of abundant gastropods and bivalves. Dense, deep bioturbation can also be present, and trough cross-stratifications are common. Facies F11 consists of grainstone to packstone with bivalves, serpulids, rare echinoderm plates and peloids. This facies is only observed in the interval between 25 and 27 m in the section. Facies F12 is composed of a peloid-bioclastic packstone with abundant bivalves, gastropods, and echinoderm plates associated with some

ammonoids and serpulids. This facies is observed at two intervals within the section (~35 m and 43.5 m). Facies F13 consists of a peloid-bioclastic wackestone to packstone. This intensely and deeply bioturbated facies is observed in two thin intervals within the section (~32 m and 37.5 m). Ammonoids are observed in three intervals within the third lithological unit (Fig. 4). *Meekoceras* is documented between 34.5 and 35 m in facies F12. The second main occurrence consists of *Guodunites* and *Churkites*, observed in facies F10 and F13, between 36.5 and 37.5 m. The uppermost occurrence of common *Anasibirites* and *Wasatchites* is observed in facies F10 between 41 and 42 m.

3.2. Beas Lewis Flats section

This section can be subdivided into four lithological units (Figs 2b, 8). The first unit, which is beyond the scope of this work, corresponds to the Permian bioclastic and bioturbated limestones of the Kaibab Formation. The base of the section displays a 20 m-thick interval composed mainly of dolomitized and silicified limestones. Only the uppermost 7 m of this lithological unit are illustrated in figure 8. An intense bioturbation emphasized by silicification is recorded in these Permian limestones. Two bioclastic-rich intervals with cross bedding are observed at about 15 m above the base of the section. These Permian limestones are also locally affected by intense karstification (Fig. 8).

The second lithological unit is 34 m thick and corresponds to the red beds of the Black Dragon Formation. These red beds (Facies F1) are similar to those observed at the base of the French Fork section. The Beas Lewis Flats section exhibits a progressive transition between the second and the third lithological units.

The ~ 6 m-thick third lithological unit corresponds to the massive peritidal limestones (F2 and F3) of the lower Sinbad Formation. This unit is only half as thick as corresponding beds in the French Fork section; it does not exhibit conspicuous m-scale patchy microbial structures. It can be subdivided into three subunits (Fig. 8). The basal subunit (between 53.5 m and 56 m) includes the first limestone beds that interfinger with the dolosiltstones (F1) of the red bed unit. These uppermost red bed intercalations are notably richer in micritic intraclasts. This first subunit is comprised of floatstone with some localized small cm- to dm-large domal stromatolites (F2; Figs 9a, 10). Rare gastropods and siliceous sponges also occur. Additionally, even though burrows could not be clearly identified, the distribution of sedimentary grains tends to record an apparent infaunal activity. The second subunit (between 56 m and 58.5 m) corresponds to relatively well-bedded limestone (F3), including 3 main subfacies (F3a-c; Fig. 10). Each bed exhibits a basal part with abundant gastropods (F3a; Figs

9b, 11). This subfacies can also be rich in intraclasts and it also includes some rare siliceous sponges (Fig. 10k–m). The middle part of these beds corresponds to fenestral limestone subfacies (F3b; Figs 10h–j, 12), and the upper part displays laminated mudstones with sheet cracks (F3c; Figs 10e–g, 11). The third subunit (between 58.5 m and 60 m) consists of oncoid-fenestral limestones (F3e) with abundant peloids and some ooids, aggregate grains, gastropods, serpulids and ostracods (Fig. 10b–d). This subfacies is characterized by large fenestrae that display internal stromatolites with upward and downward growth directions.

The fourth lithological unit of the Beas Lewis Flats section is characterized by a succession of dolostone intervals (F5) with various bioclastic, oolitic or peloidal limestones (F6-F10, F12 and F13). This bioclastic limestone unit comprises the upper 30 m of the section. From 61.5 to 65 m, two m-thick beds correspond to a peloid-intraclastic grainstone (F6). From 65 to 69.5 m, ooid-bioclastic grainstone (F8) and peloid-bioclastic grainstone (F9) are particularly well represented, interfingering with thin intervals of dolostones (F5). At about 70 m, a thin dm-thick interval of intraclastic grainstone (F7) is observed, in which subangular to angular limestone intraclasts are associated with well-rounded lithoclasts. The first occurrence of peloidal and bioclastic wackestone (F13) is documented above this intraclastic interval. From 74 m, dolostone intervals interfinger with bioclastic limestone beds of facies F10, F12 and F13. At about 78 m, specimens of the ammonoid *Anasibirites kingianus* are observed in a thin dm-thick interval within facies F13.

3.3. Pleasant Creek section

The Pleasant Creek section is subdivided into three lithological units (Fig. 12). Permian limestones of the Kaibab Formation are visible within a 15 m interval at the base of the section (Fig. 2c). These limestones are strongly dolomitized and no fossil grains could be identified. Nonetheless, some sedimentary structures are still recognizable, such as abundant planar laminations, small asymmetrical ripples, and some trough cross-bedding.

Above a stratigraphic gap of 5 m, a 15 m-thick red bed unit of the Black Dragon Formation is documented. The uppermost part of this unit corresponds to F1 that displays frequent conglomeratic intervals. Some tepee structures and desiccation cracks are also observed.

The third lithological unit corresponds to the bioclastic limestone unit of the upper Sinbad Formation. The thick microbial limestone unit of the lower Sinbad Formation observed at French Fork and Beas Lewis Flats is therefore not recorded at Pleasant Creek. In the basal 5 m, several intervals of intraclastic limestone (F2) are interfingered with dolostones

(F5). At 38.5 m, a dm-thick bed exhibits domal stromatolites (F4; Fig. 13a). Microscopically, these stromatolites consist of dense micritic laminae, which sometimes reveal desiccation cracks, alternating with fenestral laminae (Fig. 13b). From 40 to 45 m, dolostones (F5) are interfingered with dm- to m-thick peloidal-intraclastic limestones (F6). These beds display internal cross bedding, frequent mudclasts, and important changes in lateral thickness. A second occurrence of intraclastic limestones (F2) and stromatolites (F4) is recorded between 45 m and 46 m. In this case, the stromatolitic interval can be subdivided into a lower bed characterized by dm-scale wavelength domal stromatolites and an upper stratiform bed displaying a wavy laminated structure (Fig. 13c). Microscopically, these wavy microbial carbonates are comprised of an alternation of dense micritic laminae with clotted laminae (Fig. 13d).

The rest of the section is characterized by a succession of dolostones (F5) with various bioclastic, ooidal, and peloidal limestones. From 46 m to 48 m, a thick ooid-peloidal grainstone (Facies F8) displays herringbone cross-stratification in its uppermost part (Fig. 13e). It is characterized by well-sorted ooids associated with some gastropods (Fig. 13f). From 49.5 m to 52.5 m, the section displays an interval characterized by an alternation of dolostones (F5) with bioclastic facies (F10, F12, and F13). This interval is notably characterized by its intense bioturbation and the presence of echinoderm fragments (Fig. 12; Table 1). At about 55 m, an oolite-rich bed (F8) contains abundant *Anasibirites kingianus*. In the uppermost part of the section (at 57 m), some cm-scale beds with basal erosive parts are particularly rich in bivalves (F11 and F12; Fig. 13g) that exhibit siliceous sponges under their disarticulated valves (Fig. 13h).

4. FACIES MODELS AND DEPOSITIONAL ENVIRONMENTS

For the studied stratigraphic interval, the 13 identified facies can be placed into two facies models (Fig. 14; Table 1). The first model is characterized by the red beds (F1) of the Black Dragon Formation and the microbial limestones (F2 and F3) of the lower Sinbad Formation (Fig. 14a). Progressive gradation between the red bed deposits and the microbial limestones observed in the Beas Lewis Flats section supports a common facies model for these deposits. Previous workers mentioned the vertical interfingering between the Black Dragon red beds and the Sinbad carbonates (Blakey, 1974, 1977; Dean, 1981; Goodspeed and Lucas, 2007). Red beds can have originated in various depositional environments such as marginal marine,

deltaic, and coastal plain settings (Voigt *et al.*, 2013; Thomson and Lovelace, 2014). In this first depositional model, the red beds display both cm-scale planar- or ripple-bedding structures and climbing ripples that are consistent with a tide-dominated setting. Rippled siltstones and fine sandstones are interpreted as deposits of the lower intertidal (low tidal flats) to shallow subtidal zone, where bedload transport occurs during moderate tidal activity (Alam, 1995). The paucity of tidal channels in the red beds can be considered as an evidence of a low palaeotidal range (Walker and Harms, 1975). It may also indicate a gentle palaeoslope, such as a low gradient inner shelf or embayment, in which the tidal currents were not strong enough to develop tidal channels (Alam, 1995). Limestones (F2 and F3) of the lower Sinbad Formation represent a facies association interpreted as peritidal, which formed in environments around the tidal zone (Wright, 1984; Flügel, 2004). The rarity of siliciclastic grains suggests a position still under terrigenous influence, but sufficiently removed from the terrigenous sources. *In situ* and reworked desiccation cracks observed in F2 provide evidence of at least temporarily emerged small islands. Small cm-scale stromatolitic domes observed locally in this facies highlight some zones of higher accommodation, also allowing for an infaunal activity. The peritidal limestones (F3) are subdivided into five subfacies (F3a-e; Table 1). These subfacies vary both laterally and vertically in the same bed, suggesting a patchy facies distribution (facies mosaic; Wright and Burgess, 2005; Strasser and Védrine, 2009). Gastropod-rich packstone (F3a), which show important lateral thickness changes, may represent winnowed subtidal skeletal deposits in zones of gently sloping gully surfaces (Fig. 14a). These gastropods can also be found in the margin of small ponds that merged with surrounding intertidal flats (Shinn, 1969). The fenestral limestones (F3b) are the most common deposits of the peritidal facies association and represent supratidal or intertidal sediments (Shinn, 1968). With biofilms that coated numerous fenestrae and diverse grains, this subfacies commonly developed a small synoptic relief above the sea floor. Vadose silts observed in some fenestrae are consistent with areas intermittently exposed at the time of deposition. Mudstone deposits (F3c) with sheet-cracks, a restricted fauna (ostracods and gastropods), and some stromatolites reflect supratidal to intertidal low-energy settings. Ooid-oncoid-peloidal grainstone (F3d) deposited in subtidal high-energy gullies. The latter may have enhanced the patchy geometry of these peritidal deposits. Large sheet-like fenestrae limestones with oncoids and sparse ooids (F3e) are interpreted to reflect more distal shallow subtidal settings. The presence of siliceous sponges and gastropods in these peritidal limestones (F3) is also indicative of marine conditions and thus, of a seaward position of the lower Sinbad limestones as compared to the red beds of the Black Dragon Formation.

The second facies model is characterized by deposits of the bioclastic limestone unit (i.e., the upper Sinbad Formation; Fig. 14b). The 11 facies included in this model can be grouped into three facies associations typical of the following three different depositional settings: (i) tide-dominated interior platform; (ii) tide-dominated shoal complex; and (iii) open wave-dominated marine platform. Dolostones (F5) represent internal muddy and low-energy depositional settings, recording variable amount of terrigenous inputs. It differs from the red beds (F1) by recording obvious marine influences shown by the presence of bivalves, gastropods and echinoderm plates. These dolostones are consistent with deposition on a vast interior platform or a large embayment system. Stromatolites made of small domes and wavy laminated structures (F4) may have formed in upper intertidal and supratidal zones within this interior platform. Ooid-bioclastic grainstone with some bivalves (F8) is probably indicative of stronger tidal currents, and possibly wave action that impacted the shoal complex area. As observed on both the ocean-ward and platform-ward sides of the oolitic shoal, the peloid-bioclastic grainstone with bivalves and sparse ooids (F9) logically points to less vigorous tidal currents. Well-marked herringbone cross-stratifications observed in these shoal deposits (F8 and F9) indicate a tide-dominated process. Intraclastic rudstone (F7) and peloid-intraclastic limestones (F6) were deposited in channels that cut across the shoal. Seaward of the tidal-dominated shoal complex, sediments may have evolved from peloidal and ooidal sands into a mixture of skeletal (gastropods, bivalves, serpulids and echinoderms) and peloidal sands (Halley *et al.*, 1983, p. 472). More abundant bioclasts recorded in grain-supported sediments (F10 and F11) may have been deposited on the seaward side of the tide-dominated shoal complex. An inner- to mid-shelf transition zone is marked by the deposition of bioclastic packstone (F12). Mud-supported texture and intense bioturbation that characterize peloidal-bivalve wackestone (F13) indicate deposition below the fair-weather wave base in an offshore position. The record of vertically oriented bivalves in F12 and F13 suggests local turbulent and rotary flows during storms (Pérez-López and Pérez-Valera, 2011). The frequent record of ammonoids in these facies also confirms an open-ocean influence. Thus, in a large embayment system, the shoal complex can be considered as tide dominated, even if its seaward margin was impacted by open-sea waves.

5. SECTION CORRELATION AND DEPOSITIONAL SEQUENCES

The only previous attempt to correlate sections in the Torrey area was largely based on a lithostratigraphic approach (Dean, 1981). For the herein studied sections, age assignments are nevertheless possible owing to conodont and ammonoid occurrences. Conodonts from the base of the upper Sinbad Limestone at French Fork yield a Smithian age. However, no definite conodont zonation and correlation are possible between the French Fork, Beas Lewis Flats and Pleasant Creek sections. Therefore, the record of the *Anasibirites* fauna within dm-scale levels in the upper part of these three sections is the only correlation timeline available within the Torrey area (Fig. 15). Based on these *Anasibirites* beds, it is possible to recognize distinct hierarchical stacking patterns and facies evolution in the sedimentary succession, thus allowing for the identification of large-, medium-, and small-scale depositional sequences. At each hierarchical level, the facies evolution of depositional sequences generally indicates deepening and shallowing trends defined by transgressive surfaces (Strasser *et al.*, 1999).

The Black Dragon and Sinbad formations reflect a large-scale depositional sequence, which is similar to the facies evolution previously described in the San Rafael Swell area (Goodspeed and Lucas, 2007). The Black Dragon red beds, which represent clastic tidal-flat deposition (Blakey, 1974), mark the beginning of the transgressive trend. Maximum accommodation corresponds to the *Anasibirites* beds observed in the uppermost Sinbad Formation. The sequence boundary may either be at the top of the Sinbad Formation or in the lower part of the Spathian Torrey Formation, in agreement with the interpretation of Goodspeed and Lucas (2007).

Five medium-scale sequences are identified (S.I-V; Fig. 15). The first sequence is initiated at the top of the Permian limestones, but no clear facies evolution can be observed in the dolosiltstones of the red beds. The second medium-scale depositional sequence is well visible at French Fork and Beas Lewis Flats. Intraclastic limestones (F2) observed at the base of the microbial unit of the lower Sinbad Formation mark the transgressive interval of this second medium-scale depositional sequence. The sparse ammonoid record at French Fork and the presence of large fenestrae and oncoids (F3e) in the uppermost part of the microbial limestone unit at Beas Lewis Flats underline the maximum flooding interval (Figs 4, 8). This second depositional sequence is more difficult to observe at Pleasant Creek, where the microbial limestone unit is absent (Fig. 15). The progressive decrease in thickness of the microbial limestone unit between French Fork and Beas Lewis Flats and its absence in Pleasant Creek is consistent with a general retrogradational pattern of this facies toward the southeast (Dean, 1981). The erosional surface at the top of the microbial limestone unit at Beas Lewis Flats marks the sequence boundary of this second medium-scale sequence. The

remaining three medium-scale depositional sequences are characterized by a facies evolution with deepening-shallowing trends marked by a complex interplay between lower shoreface, shoal, and tidal flat deposits. Thus, the third medium-scale sequence displays a basal transgressive interval, well recorded at Pleasant Creek with stromatolitic (F4) and intraclastic (F2) deposits. The progressive incursion of seaward bioclastic shoal deposits at French Fork and of shoal complexes at Beas Lewis flats is consistent with a deepening trend. The maximum flooding interval is marked by the presence of subtidal bars made of bivalve-rich limestones (F11) at French Fork, allowing the accumulation of thick ooidic shoal deposits at Beas Lewis Flats. A thick interval of interior platform dolostones (F5) underlines the progradational trend at the end of this third medium-scale sequence. During the initiation of the deepening trend of the fourth medium-scale depositional sequence, lower shoreface deposits with ammonoids are recorded at French Fork, whereas at Beas Lewis Flats, only a thin oolitic interval is observed. In a more proximal setting, stromatolitic (F4) and intraclastic (F2) deposits mark this transgressive interval at Pleasant Creek. The record of *Anasibirites* ammonoid fauna in the three sections indicates the maximum flooding interval. The shallowing trend is characterized by the presence of ooidic shoal deposits in Pleasant Creek and then dolostones (F5), which are relatively thick at Beas Lewis Flats. The fifth medium-scale depositional sequence is well visible only at Beas Lewis Flats. Seaward bioclastic shoal deposits (F9-F12) mark the deepening trend. Offshore deposits (F13) underline the maximum flooding interval. The shallowing trend is evidenced by deposition of a thick interval of dolostones (F5), and the sequence boundary corresponds to the limit between the deposits of the Sinbad and Torrey formations.

Within such large- and medium-scale hierarchical stacking patterns, more than fifteen small-scale depositional sequences can be identified. In the middle Smithian microbial limestones of the French Fork section, five small-scale sequences can be recognized. Dm-thick intervals of thin laminated beds (F3c) or erosive surfaces delimit these sequences in which m-scale patch reefs developed (Fig. 2a). Such a stacking pattern is not observed at Beas Lewis Flats, where facies evolution reflects a medium-scale increase in accommodation (Figs 8, 10). With the change of depositional settings during the late middle to late Smithian (Fig. 14), small-scale sequences are marked by rapid facies shifts between offshore, shoal and interior platform deposits. In some intervals, correlation between these small-scale sequences is apparently possible, but for other intervals, their numbers and thicknesses differ greatly between the three studied sections, making their correlation difficult (Fig. 15).

Depositional sequences characterized by a facies evolution corresponding to the shortest recognizable cycle of environmental change are called elementary sequences (Strasser *et al.*, 1999). These elementary sequences, which generally correspond to one bed, are observed within 13 successive beds of the microbial limestone unit at Beas Lewis Flats (Fig. 11). Facies evolution of these elementary sequences involves a succession of gastropod-rich accumulations (F3a), fenestral limestones (F3b), and laminated mudstones (F3c; Fig. 11).

6. ORIGINS OF DEPOSITIONAL SEQUENCES

Global sea-level curves indicate a general rise during the Permian-Triassic transition (Haq and Al-Qahtani, 2005; Haq and Shutter, 2008). During this global trend, several world-wide localities record third order sea-level cycles in Lower Triassic rocks (Embry, 1997; Vigran *et al.*, 1998; Lehrmann *et al.*, 2001, 2007a, b). In the western USA basin, the Lower Triassic sedimentary succession records three third-order transgressive-regressive sequences, namely in the Griesbachian, Smithian and earliest-middle Spathian (Paull and Paull, 1993, 1997). In southern Utah, the Early Triassic transgression began in the early middle Smithian (Goodspeed and Lucas, 2007; Brayard *et al.*, 2013). The large-scale depositional sequence recognized in the Torrey area is consistent with this Smithian third-order sea-level cycle.

The medium-scale sequences can be correlated across the three studied sections. Indeed, they display relatively close bed-stacking patterns and facies evolution (e.g. the progressive retrogradation of offshore deposits in the bioclastic limestone unit; Fig. 15) that are congruent with a sea-level control. Based on published U/Pb ages and the comparison of average Smithian ammonoid zone durations inclusive of separation intervals (see Brühwiler *et al.*, 2010 for details), the Sinbad Formation likely represents a duration less than 490 kyr in the Torrey area. Thus, observed medium-scale depositional sequences may reflect the orbital cycle of eccentricity. The lack of a regressive trend in the second medium-scale depositional sequence coupled with the presence of a truncated surface at the top of the microbial limestone unit of the lower Sinbad Formation is consistent with a sudden drop in sea level, which may have a tectonic origin. A regional tectonic uplift probably related to the Sonoma Orogeny (Collinson *et al.*, 1976) has also been identified at the top of fenestral-microbial limestones of the Sinbad Formation in southwest Utah (Olivier *et al.*, 2014). Additionally, a local inherited topography at the top of the microbial limestone unit may also explain the formation of a thick ooidic shoal system in the Beas Lewis Flats area.

The origin of small-scale sequences is often more difficult to assess because autocyclic processes inherent in the depositional system also played a role in their formation (Strasser *et al.*, 2012). These autocyclic processes, including progradation or lateral migration of sedimentary bodies (tidal flats, shoals or delta lobes), can lead to the formation of shallowing-up depositional sequences (Ginsburg, 1971; Pratt and James, 1986; Satterley, 1996; Drummond and Wilkinson, 1993; Burgess, 2006). At Beas Lewis Flats, the upper Sinbad Formation consists of tide-dominated ooidic shoal deposits that actually reflect important lateral facies migration. Along the three studied sections, small-scale sequences show a disordered pattern and a limited lateral consistency. All these observations argue for a preponderant role by autocyclic processes rather than putative orbitally-forced sea-level changes in the formation of small-scale depositional sequences.

Observed elementary sequences reflect a facies evolution corresponding to the succession of gastropod-rich accumulations (F3a), fenestral limestones (F3b), and laminated mudstones (F3c; Fig. 11). This shortest recognizable cycle of environmental change is relatively similar to the Alpine Late Triassic Lofer (Dachstein) cycles originally described in the Austrian northern calcareous Alps (Fischer, 1964). Interpretation of these peritidal cyclic carbonate sequences is controversial. They can be interpreted as reflecting a deepening-upward cycle (Fisher, 1964), a shallowing-upward cycle (Goldhammer *et al.*, 1990, Satterley, 1996; Cozzi *et al.*, 2005), or as a structure formed in tune with autocyclic processes (Enos and Samankassou, 1998). Even though such sequences are now largely documented in Middle and Late Triassic deposits, they are generally considered as unknown in Lower Triassic sedimentary successions (Weidlich and Bernecker, 2007). However, one site in the Smithian–Spathian strata of the Great Bank of Guizhou (South China) records thrombolitic reef mounds within peritidal cyclic limestones (Lehrmann *et al.*, 1998, 2001). These deposits display a typical thrombolite-bearing parasequence – i.e., another term illustrating the fundamental building block of sequences (Mitchum and Van Wagoner, 1991) – that consists in the upward succession of a basal oolitic grainstone overlain by skeletal packstone, thrombolite reef mounds, and capped by flaser-bedded limestones. Such a parasequence (0.2 to 7.4 m-thick) has been interpreted as reflecting low-amplitude, high frequency (5^{th} order, 0.01–0.1 my) sea-level fluctuations resulting from greenhouse conditions (Lehrmann *et al.*, 2001). At Beas Lewis Flats, gastropod accumulations are laterally discontinuous, suggesting a concentration in subtidal local topographic low points. It may also represent lag deposits during phases of lateral migration of gullies (Fig. 14a). Subfacies F3b, with abundant fenestrae, some microbial deposits and sparser gastropods, represents intertidal deposits that progressively

filled available space in local ponds or abandoned gullies. Subfacies F3c, with abundant sheet cracks, some stromatolites and a restricted fauna (some ostracods and gastropods), reflects an intertidal to supratidal area prone to record intermittent exposure and desiccation. At French Fork, fenestral (F3b) and muddy laminated (F3c) subfacies are laterally observed in the same bed (Fig. 7). Such an observation, coupled with the limited lateral consistency of these subfacies between French Fork and Beas Lewis Flats, supports an autocyclic origin of the observed elementary sequences.

7. SIGNIFICANCE OF MICROBIAL DEPOSITS: ARE THEY LINKED TO DELETERIOUS ENVIRONMENTS?

It is classically assumed that a return to pre-extinction levels in taxonomic and functional diversity after the end-Permian mass extinction did not occur until the end of the Early Triassic (Schubert and Bottjer, 1995; Lehrmann *et al.*, 2006; Chen and Benton, 2012; Pietsch and Bottjer, 2014). Lower Triassic rocks are thus often considered to record low-diversity benthic faunas (Lehrmann *et al.*, 2001; Fraiser and Bottjer 2004; Pruss *et al.*, 2006). In this context, microbialites are thought to have flourished as a consequence of continuous or recurrent environmental stresses such as anoxia or high water temperature (Song *et al.*, 2014, Pietsch *et al.*, 2014) and in the absence of developed benthic faunas (Schubert and Bottjer, 1992, 1995). Indeed, several microbialite pulses have been identified in Early Triassic rocks (Baud *et al.*, 2007, Algeo *et al.*, 2011, Mata and Bottjer, 2012). It has therefore been suggested that these microbialite episodes may reflect the unusual chemistry of Early Triassic oceans (Pruss and Bottjer, 2004; Woods, 2014). However, recent studies have demonstrated that the rediversification of some nekto-pelagic organisms such as ammonoids (Brayard *et al.*, 2009b) and conodonts (Orchard, 2007) was explosive after the mass extinction. The consensual view of widespread depauperate benthic faunas throughout the entire Early Triassic is now obsolete, as shown by the diversified assemblages recently described from various time intervals and latitudes (Twitchett *et al.*, 2004; Wheeley and Twitchett, 2005; Beatty *et al.*, 2008; McGowan *et al.*, 2009; Shigeta *et al.*, 2009, Kaim *et al.*, 2010; Hautmann *et al.*, 2011, 2013; Hofmann *et al.*, 2011, 2013 a, b, 2014).

In the Torrey area, the observed lithological succession is consistent with two depositional models (middle and late middle to late Smithian, respectively; Fig. 14). The first model implies an extension of peritidal microbial limestones (F3) over tens of kilometres (see

also Dean, 1981), which laterally pass to more internal tidal-flat red beds (F1; Fig. 14a). Within these microbial limestones, the associated fauna, although common, is of relatively low diversity and is mainly represented by ostracods, gastropods, some bivalves and rare foraminifers. Such a biotic assemblage could be interpreted as representing an impoverished and low-complexity marine ecosystem, typified by primary producers and opportunistic consumers (Lehrmann *et al.*, 2001; Chen and Benton, 2012; Crasquin and Forel, 2013). In this context, microbialites are expected to be widespread and capable of forming patch reefs (Schubert and Bottjer, 1992, 1995; Lehrmann, 1999; Pruss and Bottjer, 2004). Nevertheless, at French Fork, the occurrence of frequent siliceous sponges in the reef framework confirms the existence of an advanced ecological step above microbe-only constructions early in the Early Triassic (Pruss *et al.*, 2007; Brayard *et al.*, 2011; Marenco *et al.*, 2012; Pandolfi and Kiessling, 2014; Vennin *et al.*, in press). Similar sponge-microbe reefs have already been reported from the early Smithian of central Utah (Brayard *et al.*, 2011), thus demonstrating that the Smithian occurrence is not anecdotal in the western USA basin. Their diachronous formation during the Smithian transgression also suggests that they are probably linked to water depth/energy/nutrient conditions.

The record of the Early Triassic biotic recovery appears to be strongly dependent on the type of depositional setting (Pruss *et al.*, 2006; Beatty *et al.*, 2008; Mata and Bottjer 2011; Olivier *et al.*, 2014). In the Torrey area, previous studies interpreted the sediments of the Black Dragon and Sinbad formations as part of the same depositional model (Blakey, 1974; Dean, 1981). However, high-resolution correlation between the three studied sections does not support such a lateral facies distribution between microbial limestones (F3) of the lower Sinbad Formation and the more diversified bioclastic limestones (F10-F13) of the upper Sinbad Formation (Fig. 14a and b). Such a lateral facies variation was nevertheless assumed in southwestern Utah in time-equivalent Sinbad limestones (Olivier *et al.*, 2014). The lack of a fauna in the Black Dragon Formation red beds (F1) must be considered from the perspective that these deposits formed in a tidal-system reflecting important terrigenous inputs (Fig. 14a). In such depositional settings, significant sediment mobility (caused by tidal currents) and abundant suspended sediment particles (that prevent the colonization by filter-feeding organisms) may cause intertidal settings to be prohibitive environments for common benthic organisms (Davies and FitzGerald, 2004). Indeed, the western USA basin corresponds to a narrow epicontinental shallow sea that progressively transgressed southward during the Smithian (Paull and Paull, 1993; Goodspeed and Lucas 2007; Brayard *et al.*, 2013). Abundant lower-middle Smithian terrigenous red-bed deposits in central and southern Utah indicate the

existence of complex topographic highs as well as significant continental erosion along the margins of an epicontinental sea tongue or embayment system (Blakey, 1974; Dean, 1981; Nielson, 1991; Olivier *et al.*, 2014). Thus, the intense microbial development in the lower Sinbad Formation coupled with the lack of a fauna in the contemporaneous red beds of the Black Dragon Formation may be explained by specific local environmental conditions. Microbialites are not consistent with high rates of sedimentation (Kershaw *et al.*, 1999), and therefore microbial limestones (F3) could not have formed very close to the terrigenous sources where the red beds were deposited. On the other hand, associated with the terrigenous flux in marine systems, nutrient-rich conditions may have appeared, thus favouring the formation of microbial deposits (Dupraz and Strasser, 2002; Olivier *et al.*, 2004). Red beds were favoured by an intense weathering of silicate rocks, which could have increased the amount of carbonate minerals delivered to the oceans (Ferris et al., 1994; Locklair and Lerman, 2005). Carbonate precipitation depends on carbonate alkalinity and the availability of free calcium (Dupraz and Visscher, 2005; Aloisi, 2008). The intense erosion of calcareous Permian deposits of the Kaibab Formation also supports the existence of seawaters enriched in Ca^{2+} (Arp *et al.*, 2003). Coupled with the rare skeletal carbonate sinks during the middle Smithian, a shift in the carbonate saturation of seawater can help to explain the intense development of microbialites (Pruss *et al.*, 2005; Payne *et al.*, 2007). Thus, the formation of middle Smithian microbial deposits in the lower Sinbad Formation may have occurred in a specific depositional window corresponding to a peritidal setting sufficiently distant from terrigenous sources but still under the influence of alkaline and/or nutrient-rich waters.

During the late-middle to late Smithian, the depositional environment changed drastically. Faunas, which are notably more abundant and diversified, include bivalves, gastropods, echinoderms, ammonoids and serpulids. An intense infaunal activity is also recorded (Fig. 14b). This environmental change may be explained by an acceleration of the transgression following a significant sea-level drop of probable tectonic origin at the top of the microbial limestone unit. The inherited topography probably allowed the formation of an oolitic shoal complex in the Beas Lewis Flats area (Fig. 15). It also permitted recurrent incursions of seaward shoal complex deposits characterized by a more diversified fauna. These ooid-bioclastic limestones comprise the upper Sinbad Limestone Formation. This unit exhibits a relatively high diversity and abundant fauna up to the *Anasibirites kingianus* beds (Brayard *et al.*, 2013; Pietsch *et al.*, 2014, Hofmann *et al.*, 2014). These bioclastic limestones (F10-13) interfinger with intertidal interior platform dolostones (F5) that contain a sparse and poorly preserved fauna. In the upper Sinbad facies model (Fig. 14b), microbial deposits are

still documented, but their nature and depositional setting strongly differ from their lower Sinbad counterparts. In the youngest case, dm-thick beds of domal stromatolites or wavy carbonate structures (F4) display a laminated micritic fabric. Such microbial carbonates may have played a stabilizing role on the internal part of the shoal complex such as do modern seagrass communities (Rankey, 2014). However, modern and ancient microbialites observed near high-energy shoals incorporate sand-size detrital particles (Riding *et al.*, 1991; Feldmann and McKenzie 1998; Planavsky and Ginsburg, 2009). Fine-grained microbial deposits closely associated with high-energy shoals are known in the Middle Jurassic and they are interpreted as being deposited in tune with sea-level fluctuations (Tomás *et al.*, 2013). This is not the case in the Torrey area where depositional sequences, including microbial, oolitic and dolostone deposits, are better explained by autocyclic processes. Early Triassic wrinkle structures have also been described associated with cross-laminated siltstones interbedded with shales on supratidal flat environments (Hips, 1998, Pruss *et al.*, 2004; Mata and Bottjer, 2012). Late middle to late Smithian dolostones (F5) in the Torrey area reflect a tide-dominated interior platform with minor terrigenous influences. Thus, observed wavy microbial carbonates can display structures similar to their wrinkle siliciclastic analogues. However, since they formed in a mud-dominated setting, they could not have integrated siliciclastic grains (Luo *et al.*, 2013). Observed wavy microbial carbonates may therefore reflect local low-energy topographic highs in the interior platform, whereas dm-scale domal stromatolites probably formed in an area characterized by a slightly higher accommodation (Fig. 14b). All of these microbial limestones (F4) are clearly contemporaneous with the more distal and more diversified bioclastic limestones (F10-13) of the upper Sinbad Formation. They can be considered as reflecting marine and oxic waters, as previously suggested for younger Spathian microbialites in the Virgin Limestone Formation in western USA (Schubert and Bottjer, 1992, 1995). Thus, both lower and upper Sinbad microbialites (F3 and F4) observed in the Torrey area indicate that Early Triassic microbialites were able to form in various depositional settings that did not necessarily reflect deleterious environments.

8. CONCLUSIONS

The lithological succession in the Torrey area represents a general transgression after the Permian-Triassic mass extinction. This transgression corresponds to the middle Smithian 3rd order sea-level cycle. The stacking pattern of the studied stratigraphical interval allows the

identification of large, medium, small-scale and elementary depositional sequences. While one particular medium-scale depositional sequence observed in the lower Sinbad Formation (middle Smithian) may reflect a regional tectonic uplift, others possibly formed in tune with orbitally (eccentricity) controlled sea-level fluctuations within the upper Sinbad Limestone Formation (late middle to late Smithian). Autocyclic processes better explain small-scale and elementary depositional sequences.

During the Smithian, the sedimentary systems documented in the Torrey area show depositional settings characteristic of an embayment or a sea tongue. The sedimentation reflects a tide-dominated regime that displays wave influences only during major phases of transgression. The first depositional model highlights the juxtaposition between the Black Dragon (red beds) and Lower Sinbad formations, corresponding to a siliciclastic tidal flat and peritidal microbial limestones, respectively. Microbial limestones developed m-scale patch reefs and display a rather low-diversity benthic fauna with gastropods, ostracods, rare foraminifers, and common siliceous sponges. The contribution of siliceous sponges to the reef framework indicates an advanced ecological step above microbial-only reefs. Similar sponge-microbe associations were also documented from older beds of the early Smithian of central Utah, indicating that these bioconstructions were probably common within the western USA basin. The second upper Sinbad depositional model is characterized by three main facies associations: (i) tidal flat dolostones of the interior platform; (ii) ooid-bioclastic deposits of a tide-dominated shoal complex; and (iii) bioclastic limestones of open wave dominated marine settings.

Microbialites occur in both lower and upper Sinbad depositional models. During deposition of the lower Sinbad, the initiation of the transgression allowed the development of a large microbial-dominated peritidal area seaward of a siliciclastic tidal flat in which red beds devoid of any fauna were being deposited. The formation of these microbialites seems to have occurred in a specific depositional window sufficiently far from terrigenous sources, but still under the influence of alkaline and/or nutrient-rich waters. During the upper Sinbad deposition, the sea-level rise permitted the formation of a mixed wave-tide dominated sedimentary system and the microbialitic growth was limited to a small area in the dolostone interior platform. A rather low-diversity fauna characterizes the lower Sinbad microbial deposits, whereas upper Sinbad stromatolites are contemporaneous with a much more diversified and abundant fauna. The nature of microbialites and their formation apparently depend strongly on the type of depositional setting. These Smithian microbialites do not

reflect the peculiar deleterious environmental conditions that are classically assumed for the Early Triassic time interval.

ACKNOWLEDGEMENTS

This work is a contribution to the ANR project AFTER (ANR-13-JS06-0001-01). The Région Bourgogne and the CNRS INSU Interrvie also supported this study. N. Goudemand (Zurich) is thanked for his help with conodont determinations. D.A. Stephen is grateful for the ongoing financial support of the College of Science & Health at Utah Valley University. Beas Lewis Flats and French Fork sections are located on US public land under the stewardship of the Bureau of Land Management (BLM) of the US Department of the Interior, their management and access to these lands is much appreciated. The Pleasant Creek section is located in Capitol Reef National Park, and was studied and collected under Permit # CARE-2013-SCI-0005, thanks to Sandy Borthwick for her help with the permitting process. Pedro Marenco and Spencer G. Lucas are thanked for their helpful comments on the manuscript.

REFERENCES

Aitken, J.D. 1967. Classification and environmental significance of cryptalgal limestones and dolomites with illustrations from the Cambrian and Ordovician of southwestern Alberta. *Journal of Sedimentary Petrology* **37,** 1163–1178.

Alam, M.M. 1995. Tide-dominated sedimentation in the Upper Tertiary succession of the Sitapahar anticline, Bangladesh. In: *Tidal Signatures in Modern and Ancient Sediments*, Flemming, B.W., Bortholoma, A. (eds). International Association of Sedimentologists, Special Publication **24,** 329–341.

Algeo, T., Kuwahara, K., Sano, H., Bates, S., Lyons, T., Elswick, E., Hinnov, L., Ellwood, B., Moser, J., Maynard, J. 2011. Spatial variation in sediment fluxes, redox conditions, and productivity in the Permian–Triassic Panthalassic Ocean. *Palaeogeography, Palaeoclimatology, Palaeoecology* 308, 65–83.

Aloisi, G. 2008. The calcium carbonate saturation state in cyanobacterial mats throughout Earth's history. *Geochimica and Cosmochimica Acta* **72,** 6037–6060.

Arp, G., Reimer, A., Reitner, J. 2001. Photosynthesis-induced biofilm calcification and calcium concentrations in Phanerozoic oceans. *Science* **292,** 1701–1704.

Arp, G., Reimer, A., Reitner, J. 2003. Microbialite formation in seawater of increased alkalinity, Satonda Crater Lake, Indonesia. *Journal of Sedimentary Research* **73,** 105–127.

Baud, A., Cirilli, S., Marcoux, J., 1997. Biotic response to mass extinction: the lowermost Triassic microbialites. *Facies* **36,** 238–242.

Baud, A., Richoz, S., Pruss, S.B. 2007. The Lower Triassic anachronistic carbonate facies in space and time. *Global and Planetary Change* **55,** 81–89.

Beatty, T.W., Zonneveld, J.P., Henderson, C.M. 2008. Anomalously diverse Early Triassic ichnofossil assemblages in northwest Pangea: a case for a shallow-marine habitable zone. *Geology* **36,** 771–774.

Blakey, R.C. 1974. Stratigraphic and depositional analysis of the Moenkopi Formation, Southeastern Utah. *Utah Geological and Mineral Survey Bulletin* **104,** 1–81.

Blakey, R.C. 1977. Petroliferous lithosomes in the Moenkopi Formation, Southern Utah. *Utah Geology* **4,** 67–84.

Brayard, A., Brühwiler, T., Bucher, H., Jenks, J. 2009a. *Guodunites* a low-palaeolatitude and trans-panthalassic Smithian (Early Triassic) ammonoid genus. *Palaeontology* **52,** 471–481.

Brayard, A., Escarguel, G., Bucher, H., Monnet, C., Brühwiler, T., Goudemand, N. Galfetti, T., Guex, J. 2009b. Good genes and good luck: ammonoid diversity and the end-Permian mass extinction. *Science* **325,** 1118–1121.

Brayard, A., Vennin, E., Olivier, N., Bylund, K.G., Jenks, J., Stephen, D.A., Bucher, H., Hofmann, R., Goudemand, N., Escarguel, G. 2011. Transient metazoan reefs in the aftermath of the end-Permian mass extinction. *Nature Geoscience* **4,** 693–697.

Brayard, A., Bylund, K.G., Jenks, J., Stephen, D., Olivier, N., Escarguel, G., Fara, E., Vennin, E. 2013. Smithian ammonoid faunas from Utah: implications for Early Triassic biostratigraphy, correlation and basinal paleogeography. *Swiss Journal of Palaeontology* **132,** 141–219.

Brühwiler, T., Goudemand, N., Galfetti, T., Bucher, H., Baud, A, Ware, D., Hermann, E., Hochuli, P.A., Martini, R. 2009. The Lower Triassic sedimentary and carbon isotope records from Tulong (South Tibet) and their significance for Tethyan palaeoceanography. *Sedimentary Geology* **222,** 314–332.

Brühwiler, T., Bucher, H., Brayard, A., Goudemand, N. 2010. High-resolution biochronology and diversity dynamics of the Early Triassic ammonoid recovery: The

Smithian faunas of the Northern Indian Margin. *Palaeogeography, Palaeoclimatology, Palaeoecology* **297,** 491–501.

Burgess, P.M. 2006. The signal and the noise: forward modeling of allocyclic and autocyclic processes influencing peritidal carbonate stacking patterns. *Journal of Sedimentary Research* **76,** 962– 977.

Chen, Z.Q., Benton, M.J. 2012. The timing and pattern of biotic recovery following the end-Permian mass extinction: *Nature Geoscience* **5,** 375–383.

Chen, Z.Q., Tong, J., Kaiho, K., Kawahata, H. 2007. Onset of biotic and environmental recovery from the end-Permian mass extinction within 1–2 million years: a case study of the Lower Triassic of the Meishan section, south China. *Palaeogeography, Palaeoclimatology, Palaeoecology* **252,** 176–187.

Collinson, J.W., Hasenmueller, W.A. 1978. Early Triassic paleogeography and biostratigraphy of the Cordilleran miogeosyncline. In *Mesozoic paleogeography of the West-Central United States*, Reynolds, A., Dolly, E.D. (eds). Society of Economic Paleontologists and Mineralogists, Pacific Coast Paleogeography Symposium **2,** 175–186.

Collinson, J.W., Kendall, C.G.S.C., Marcantel, J. B. 1976. Permian-Triassic boundary in eastern Nevada and west-central Utah. *Bulletin of the Geological Society of America* **87,** 821–824.

Cozzi A, Hinnov LA, Hardie L.A. 2005. Orbitally forced Lofer cycles in the Dachstein Limestone of the Julian Alps (northeastern Italy). *Geology* **33,** 789–792.

Davis, R., Fitzgerald, D.M. 2004. *Beaches and Coasts.* Wiley-Blackwell: New York.

Dean, J.S. 1981. Carbonate petrology and depositional environments of the Sinbad Limestone Member of the Moenkopi Formation in the Teasdale Dome Area, Wayne and Garfield Counties, Utah. *Brigham Young University Geology Studies* **28,** 19–51.

Drummond, C.N. Wilkinson, B.H. 1993. Carbonate cycle stacking patterns and hierarchies of orbitally forced eustatic sea level change. *Journal of sedimentary petrology* **63,** 369–377.

Dupraz, C., Strasser, A. 2002. Nutritional modes in coral-microbialite reefs (Jurassic, Oxfordian, Switzerland): evolution of trophic structure as a response to environmental change. *Palaios* **17,** 449–471

Dupraz, C., Visscher, P.T. 2005. Microbial lithification in marine stromatolites and hypersaline mats. *Trends in Microbiology* **13,** 429–438.

Embry, A.F. 1997. Global sequence boundaries of the Triassic and their identification in the western Canada sedimentary basin. *Canadian Petroleum Geology Bulletin* **45,** 415–433.

Enos, P., Samankassou, E. 1998. Lofer cyclothems revisited (Late Triassic, Northern Alps, Austria). *Facies* **38,** 207–228.

Erwin, D.H. 2006. *Extinction. How Life on Earth nearly ended 250 million years ago*. Princeton University Press: New York.

Feldmann, M., McKenzie, J.A. 1998. Stromatolite-thrombolite associations in a modern environment, Lee Stocking Island, Bahamas. *Palaios* **13,** 201– 212.

Ferris, G.F., Wiese, R.G., Fyfe, W.S. 1994. Precipitation of carbonate minerals by microorganisms: implications for silicate weathering and the global carbon dioxide budget. *Geomicrobiology Journal* **12,** 1–13.

Fischer, A.G. 1964. The Lofer cyclothems of the Alpine Triassic. In: Merrian, D.F. (Ed.), Symposium on cyclic sedimentation. *Kansas Geological Survey, Bulletin* **23.** 107–149.

Flügel, E. 2004. *Microfacies of carbonate rocks.* Springer: Berlin.

Fraiser, M.L., Bottjer, D.J. 2004. The non-actualistic Early Triassic gastropod fauna: A case study of the Lower Triassic Sinbad Limestone Member. *Palaios* **19,** 259–275.

Galfetti, T., Bucher, H., Ovtcharova, M., Schaltegger, U., Brayard, A., Brühwiler, T., Goudemand, N., Weissert, H., Hochuli, P.A., Cordey, F., Guodun, K. 2007. Timing of the Early Triassic carbon cycle perturbations inferred from new U–Pb ages and ammonoid biochronozones. *Earth and Planetary Science Letters* **258,** 593–604.

Galfetti, T., Bucher, H., Martini, R., Hochuli, P.A.H., Weissert, H., Crasquin-Soleau, S., Brayard, A., Goudemand, N., Brühwiler, T., Guodun K. 2008. Evolution of Early Triassic outer platform paleoenvironments in the Nanpanjiang Basin (South China) and their significance for the biotic recovery. *Sedimentary Geology* **204,** 36–60.

Ginsburg, R.N. 1971. Landward movement of carbonate mud: new model for regressive cycles in carbonates (abstract). *American Association of Petroleum Geologist, Bulletin* **55,** 340.

Goldhammer, R.K., Dunn, P.A., Hardie, L.A. 1990. Depositional cycles, composite sea-level changes, cycle stacking patterns, and the hierarchy of stratigraphic forcing: examples from Alpine Triassic platform carbonates. *Geological Society of America, Bulletin* **102,** 535–562.

Goodspeed, T.H., Lucas, S.G. 2007. Stratigraphy, sedimentology, and sequence stratigraphy of the Lower Triassic Sinbad Formation, San Rafael Swell, Utah. *New Mexico Museum of Natural History and Science Bulletin* **40,** 91–101.

Grasby, S.E., Beauchamp, B., Embry, A., Sanei, H. 2013. Recurrent Early Triassic ocean anoxia. *Geology* **41,** 175–178.

Guex, J., Hungerbühler, A., Jenks, J.F., O'Dogherty, L., Atudorei, V., Taylor, D.G., Bucher, H., Bartolini, A. 2010. Spathian (Lower Triassic) ammonoids from western USA (Idaho, California, Utah and Nevada). *Mémoires de Géologie de Lausanne* **49,** 1–81.

Halley, R.B., Harris, P.M., Hine, A.C. 1983. Bank margin environment. In: *Carbonate depositional environments,* Scholle P.A., Bebout, D.G., Moore, C.H. (eds). American Association of Petroleum Geologists Memoir **33,** 464–506.

Haq, B.U., Al-Qahtani, A.M. 2005. Phanerozoic cycles of sea-level change on the Arabian Platform. *Geoarabia* **10,** 127–60.

Haq, B.U., Shutter, S.R. 2008. A chronology of Paleozoic sea-level changes. *Science* **322,** 64–68.

Hautmann, M., Bucher, H., Brühwiler, T., Goudemand, N., Kaim, A., Nützel, A. 2011. An unusually diverse mollusc fauna from the earliest Triassic of south China and its implications for benthic recovery after the end-Permian biotic crisis: *Geobios* **44,** 71–85.

Hautmann, M., Smith, A.B., McGowan, A.J., Bucher, H. 2013. Bivalves from the Olenekian (Early Triassic) of south-western Utah: systematics and evolutionary significance. *Journal of Systematic Palaeontology* **11,** 263–293.

Hips, K. 1998. Lower Triassic storm-dominated ramp sequence in northern Hungary: an example of evolution from homoclinal through distally steepened ramp to Middle Triassic flat-topped platform. In: *Carbonate Ramps,* Wright, V.P., Burchette, T.P. (eds). Geological Society, London, Special Publication **149,** 315–338.

Hofmann, R., Goudemand, N., Wasmer, M., Bucher, H., Hautmann, M. 2011. New trace fossil evidence for an early recovery signal in the aftermath of the end-Permian mass extinction. *Palaeogeography, Palaeoclimatology, Palaeoecology* **310,** 216–226.

Hofmann, R., Hautmann, M., Bucher. H. 2013a. A new paleoecological look at the Dinwoody Formation (Lower Triassic, Western U.S.): intrinsic versus extrinsic controls on ecosystem recovery after the end-Permian mass extinction. *Journal of Paleontology* **87,** 854–880.

Hofmann, R., Hautmann, M., Wasmer, M., Bucher, H. 2013b. Palaeoecology of the Virgin Formation (Utah, USA) and its implications for the Early Triassic recovery. *Acta Palaeontologica Polonica* **58,** 149–173.

Hofmann, R., Hautmann, M., Brayard, M., Nützel, A., Bylund, K.G., Jenks, J.F., Vennin, E., Olivier, N., Bucher, H. 2014. Recovery of benthic marine communities from the end-Permian mass extinction at the low latitudes of eastern Panthalassa. *Palaeontology* **57**, 547–589.

Kaim, A., Nützel, A., Bucher, H., Brühwiler, T., Goudemand, N., 2010. Early Triassic (Late Griesbachian) gastropods from South China (Shanggan, Guangxi). *Swiss Journal of Geosciences* **103,** 121–128.

Kershaw, S., Zhang, T., Lan, G. 1999. A ?microbialite carbonate crust at the Permian–Triassic boundary in South China, and its paleoenvironmental significance. *Palaeogeography, Palaeoclimatology, Palaeoecology* **146,** 1–18.

Kershaw, S., Crasquin, S., Li, Y., Collin, P.Y., Forel, M.B., Mu, X., Baud, A., Wang, Y., Xie, S., Guo, L., Maurer, F. 2012. Microbialites and global environmental change across Permian–Triassic boundary: a synthesis. *Geobiology* **10,** 25–47.

Komatsu, T., Naruse, H., Shigeta, Y., Takashima, R., Maekawa, T., Dang, H.T., Dinh, T.C., Nguyen, P.D., Nguyen, H.H., Tanaka, G., Sone M. 2014. Lower Triassic mixed carbonate and siliciclastic setting with Smithian–Spathian anoxic to dysoxic facies, An Chau basin, northeastern Vietnam. *Sedimentary Geology* **300,** 28–48.

Krystyn, L., Richoz, S., Baud, A., Twitchett, R.J. 2003. A unique Permian–Triassic boundary section from the Neotethyan Hawa- sina basin, central Oman mountains. *Palaeogeography, Palaeoclimatology, Palaeoecology* **191,** 329–344.

Kummel, B. JR. 1954. Triassic stratigraphy of southeastern Idaho and adjacent areas. *U.S. Geological Survey Professional Paper* **254-H,** 165–194.

Lehrmann, D.J., Wei, J., Enos, P. 1998. Controls on facies architecture of a large Triassic carbonate platform: the Great Bank of Guizhou, Nanpanjiang Basin, South China. *Journal of Sedimentary Research* **68,** 311–326.

Lehrmann, D.J., Wang, Y., Wei, J., Yu, Y.Y., Xiao, J. 2001. Lower Triassic peritidal cyclic limestone: an example of anachronistic carbonate facies from the Great Bank of Guizhou, Nanpanjiang Basin, Guizhou province, South China. *Palaeogeography, Palaeoclimatology, Palaeoecology* **173,** 103–123.

Lehrmann, D.J., Ramezani, J., Bowring, S.A., Martin, M.W., Montgomery, P., Enos, P., Payne, J.L., Orchard, M.J., Wang, H., Wei, J. 2006. Timing of recovery from the end-Permian extinction: Geochronologic and bio- stratigraphic constraints from south China. *Geology* **34,** 1053–1056.

Lehrmann, D.J., Pei, D.H., Enos, P., Minzoni, M., Ellwood, B.B., Orchard, M.J., Zhang, J.Y., Wei, J.Y., Dillett, P., Koenig, J., Steffen, K., Druke, D., Druke, J., Kessel, B., Newkirk, T. 2007a. Impact of differential tectonic subsidence on isolated carbonate platform evolution: Triassic of the Nanpanjiang Basin, south China. *American Association of Petroleum Geologists, Bulletin* **91,** 287–320.

Lehrmann, D.J., Payne, J.L., Donghong, P., Enos, P., Druke, D., Steffen, K., Jinan, Z., Jiayong, W., Orchard, M.J., Ellwood, B. 2007b. Record of the end-Permian extinction and Triassic biotic recovery in the Chongzuo-Pingguo platform, southern Nanpanjiang basin, Guangxi, south China. *Palaeogeography, Palaeoclimatology, Palaeoecology* **252,** 200–217.

Locklair, R.E., Lerman, A. 2005. A model of Phanerozoic cycles of carbon and calcium in the global ocean: Evaluation and constraints on ocean chemistry and input fluxes. *Chemical Geology* **217,** 113–126.

Lucas, S.G., Goodspeed, T.H., Estep, J.W. 2007. Ammonoid biostratigraphy of the Lower Triassic Sinbad Formation, East- Central Utah. *New Mexico Museum of Natural History and Science Bulletin* **40,** 103–108.

Luo, M., Chen, Z.Q., Hu, S., Zhang, Q., Benton, M.J., Zhou, C., Wen, W., Huang, J.Y. 2013. Carbonate reticulated ridge structures from the lower Middle Triassic of the Luoping area, Yunnan, southwestern China: Geobiologic features and implications for exceptional preservation of the Luoping Biota: *Palaios* **28,** 541–551.

Marenco, P.J., Griffin, J.M., Fraiser, M.L., Clapham, M.E. 2012. Paleoecology and geochemistry of Early Triassic (Spathian) microbial mounds and implications for anoxia following the end-Permian mass extinction. *Geology* **40,** 715–718.

Mata, S.A., Bottjer, D.J. 2011. Origin of Lower Triassic microbialites in mixed carbonate-siliciclastic successions: ichnology, applied stratigraphy, and the end-Permian mass extinction. *Palaeogeography, Palaeoclimatology, Palaeoecology 300,* 158–178.

Mata, S.A., Bottjer, D.J. 2012. Microbes and mass extinctions: paleoenvironmental distri bution of microbialites during times of biotic crisis. *Geobiology* **10,** 3–24.

Mitchum, R.M., Van Wagoner, J.C. 1991. High-frequency sequences and their stacking patterns: sequence-stratigraphic evidence of high-frequency eustatic cycles. *Sedimentary Geology* **70,** 131–160.

Nielson, R.L. 1991. Petrology, sedimentology and stratigraphic implications of the Rock Canyon conglomerate, southwestern Utah. *Utah Geological Survey, Miscellaneous Publication* **91,** 1–65.

Olivier, N., Carpentier, C., Martin-Garin, B., Lathuilière, B., Gaillard, C., Ferry, S., Hantzpergue, P., Geister, J. 2004. Coral-microbialite reefs in pure carbonate versus mixed carbonate-siliciclastic depositional environments: the example of the Pagny-sur-Meuse section (Upper Jurassic, northeastern France). *Facies* **50,** 229–255.

Olivier, N., Brayard, A., Fara, E., Bylund, K.G., Jenks, J. F., Vennin, E., Stephen, D.A., Escarguel, G. 2014. Smithian Shoreline migrations and depositional settings in Timpoweap Canyon (Early Triassic, Utah, USA). *Geological magazine* **151,** 938–955.

Orchard, M. J. 2007. Conodont diversity and evolution through the latest Permian and Early Triassic upheavals. *Palaeogeography, Palaeoclimatology, Palaeoecology* **252,** 93–117.

Pandolfi, J.M., Kiessling, W. 2014. Gaining insights from past reefs to inform understanding of coral reef response to global climate change. *Current Opinion in Environmental Sustainability* **7,** 52–58.

Paull, R.A., Paull, R.K. 1993. Interpretation of Early Triassic nonmarine-marine relations, Utah, U.S.A. *New Mexico Museum of Natural History and Science Bulletin* **3,** 403–409.

Paull, R.K., Paull, R.A. 1997. Transgressive conodont faunas of the early Triassic: an opportunity for correlation in the Tethys and the circum-Pacific. In: *Late Palaeozoic and Early Mesozoic Circum-Pacific Events and their Global Correlation,* Dickins, J.M., Zunyi, Y., Hongfu, Y., Lucas, S.G., Acharyya S.K. (eds). Cambridge University Press, World and Regional Geology **10,** 158–167.

Payne, J.L., Lehrmann, D.J., Wei, J., Orchard, M.J., Schrag, D.P., Knoll, A.H. 2004. Large perturbations of the carbon cycle during recovery from the end-Permian extinction. *Science* **305,** 506–509.

Payne, J.L., Lehrmann, D.J., Follett, D., Seibel, M., Kump, L.R., Riccardi, A., Altiner, D., Sano, H., Wei, J. 2007. Erosional truncation of uppermost Permian shallow-marine carbonates and implications for Permian–Triassic boundary events. *Geological Society of America, Bulletin* **119,** 771–784.

Pérez-López, A., Pérez-Valera, F. 2011. Tempestite facies model for the epicontinental Triassic carbonates of the Betic Cordillera (southern Spain). *Sedimentology* **59,** 646–78.

Pietsch, C., Bottjer, D.J. 2014. The importance of oxygen for the disparate recovery patterns of the benthic macrofauna in the Early Triassic. *Earth Science Reviews* **137**, 65–84.

Pietsch, C., Mata, S.A., Bottjer, D.J. 2014. High temperature and low oxygen perturbations drive contrasting benthic recovery dynamics following the end-Permian mass extinction. *Palaeogeography, Palaeoclimatology, Palaeoecology* **399**, 98–113.

Planavsky, N., Ginsburg, R.N. 2009. Taphonomy of modern marine Bahamian microbialites. *Palaios* 24, 5–17.

Pratt, B.R., James, N.P. 1986. The St George Group (Lower Ordovician) of western Newfoundland: tidal flat island model for carbonate sedimentation in shallow epeiric seas. *Sedimentology* **33,** 313–343.

Pruss S.B., Bottjer D.J. 2004. Late Early Triassic microbial reefs of the western United States: a description and model for their deposition in the aftermath of the end-Permian mass extinction. *Palaeogeography, Palaeoclimatology, Palaeoecology* **211,** 127–137.

Pruss, S.B., Fraiser, M., Bottjer, D.J. 2004. Proliferation of Early Triassic wrinkle structures: implications for environ- mental stress following the end-Permian mass extinction. *Geology* **32,** 461–464.

Pruss, S.B., Corsetti, F.A., Bottjer, D.J. 2005. The unusual sedimentary rock record of the Early Triassic: A case study from the southwestern United States. *Palaeogeography, Palaeoclimatology, Palaeoecology* **222,** 33–52.

Pruss, S.B., Bottjer, D.J., Corsetti, F.A., Baud, A. 2006. A global marine sedimentary response to the End-Permian mass extinction: examples from southern Turkey and the western United States. *Earth-Science Reviews* **78,** 193–206.

Pruss, S.B., Payne, J.L. Bottjer, D.J. 2007. *Placunopsis* bioherms: the first metazoan buildups following the End-Permian mass extinction. *Palaios* **22,** 17–23.

Rankey, E.C. 2014. Contrasts between wave- and tide-dominated oolitic systems: Holocene of Crooked–Acklins Platform, southern Bahamas. *Facies* **60**, 405–428.

Raup, D.M. 1979. Size of the Permo-Triassic bottleneck and its evolutionary implications. *Science* **206,** 217–218.

Riding, R., Braga, J.C., Martín, J.M. 1991. Oolite stromatolites and thrombolites, Miocene, Spain: analogues of Recent giant Bahamian examples. *Sedimentary Geology* **71,** 121–127.

Sano, H., Onoue, T., Orchard, M., Martini R. 2012. Early Triassic peritidal carbonate sedimentation on a Panthalassan seamount: the Jesmond succession, Cache Creek Terrane, British Columbia, Canada. *Facies* **58,** 113-130.

Satterley, A.K. 1996. The interpretation of cyclic successions of the Middle and Upper Triassic of the Northern and Southern Alps. *Earth-Science Reviews* **40,** 181–207.

Schubert, J.K., Bottjer, D.J. 1992. Early Triassic stromatolites as post-mass extinction disaster forms. *Geology* **20,** 883–886.

Schubert, J.K., Bottjer, D.J. 1995. Aftermath of the Permian-Triassic mass extinction event: Paleoecology of Lower Triassic carbonates in the western USA. *Palaeogeography, Palaeoclimatology, Palaeoecology* **116,** 1–39.

Shinn, E.A. 1968. Practical significance of birdseye structures in carbonate rocks. *Journal of Sedimentary Petrology* **38,** 215–223.

Shinn, E.A. 1969. Anatomy of modern carbonate tidal-flat, Andros Island, Bahamas. *Journal of Sedimentary Petrology* **39,** 1202–1228.

Song, H., Wignall, P.B., Chu, D., Tong, J., Sun, Y., Song, H., He, W., & Tian, L. 2014. Anoxia/high temperature double whammy during the Permian-Triassic marine crisis and its aftermath. *Scientific Report* **4,** 4132.

Stewart, J.H., Poole, F.G., Wilson, R.F. 1972. Stratigraphy and origin of the Triassic Moenkopi formation and related strata in the Colorado Plateau region. *Geological Survey Professional Paper* **691,** 1–195.

Strasser, A., Védrine, S. 2009. Controls on facies mosaics of carbonate platforms: a case study from the Oxfordian of the Swiss Jura. *International Association of Sedimentologists, Special Publication*. **41,** 199–213.

Strasser, A., Pittet, B., Hillgärtner, H., Pasquier, J.B. 1999. Depositional sequences in shallow carbonate-dominated sedimentary systems: concepts for a high-resolution analysis. *Sedimentary Geology* **128,** 201–221.

Strasser, A., Védrine, S., Stienne, N. 2012. Rate and synchronicity of environmental changes on a shallow carbonate platform (Late Oxfordian, Swiss Jura Mountains). *Sedimentology* **59,** 185–211.

Thomson, T.J., Lovelace, D.M. 2014. Swim track morphotypes and new track localities from the Moenkopi and Red Peak formations (Lower-Middle Triassic) with preliminary interpretations of aquatic behaviors. In: *Fossil footprints of western North America*, Lockley, M.G., Lucas, S.G. (eds). NMMNHS Bulletin **62,** 103–128.

Tomás, S., Homann, M., Mutti, M., Amour, F., Christ, N., Immenhauser, A., Agar, S.M., Kabiri, L. 2013. Alternation of microbial mounds and ooid shoals (Middle Jurassic, Morocco): response to paleoenvironmental changes. *Sedimentary Geology* **294,** 68–82.

Twitchett, R.J., Krystyn, L., Baud, A., Wheeley, J.R., Richoz, S. 2004. Rapid marine recovery after the end-Permian mass-extinction event in the absence of marine anoxia. *Geology* **32,** 805–808.

Vennin, E., Olivier, N., Brayard, A., Bour, I., Thomazo, C., Escarguel, G., Fara, E., Bylund, K.G., Jenks, J.F., Stephen, D.A., Hofmann, R. (in press). Microbial deposits in the aftermath of the end-Permian mass extinction: a diverging case from Mineral Mountains (Utah, USA). *Sedimentology*.

Vigran, J.O., Mangerud, G., Mørk, A., Bugge, T., Weitschat, W. 1998. Biostratigraphy and sequence stratigraphy of the Lower and Middle Triassic deposits from the Svalis Dome, central Barents Sea, Norway. *Palynology* **22,** 89–141.

Voigt, S., Lucas, S.G., Krainer, K. 2013. Coastal-plain origin of trace-fossil bearing red beds in the Early Permian of Southern New Mexico, U.S.A. *Palaeogeography, Palaeoclimatology, Palaeoecology* **369,** 323–334.

Walker R.G., Harms, J.C. 1975. Shorelines of weak tidal activity: Upper Devonian Catskill Formation; Central Pennsylvania. In: *Tidal deposits: a casebook of recent examples and fossil counterparts,* Ginsburg, R.N. (ed). Springer-Verlag: New-York. 103–108.

Weidlich, O., Bernecker, M. 2007. Differential severity of Permian-Triassic environmental changes on Tethyan shallow-water carbon- ate platforms. *Global and Planetary Change* **55,** 209–235.

Woods, A.D. 2013. Microbial ooids and cortoids from the Lower Triassic (Spathian) Virgin Limestone, Nevada, USA: evidence for an Early Triassic microbial bloom in shallow depositional environments. *Global and Planetary Change* **105,** 91–101.

Woods, A.D. 2014. Assessing Early Triassic paleoceanographic conditions via unusual sedimentary fabrics and features. *Earth-Science Reviews* **137**, 6–18.

Wright, V.P. 1984. Peritidal carbonate facies models: A review. *Geological Journal* **19,** 309–325.

Wright, V.P., Burgess, P.M. 2005. The carbonate factory continuum, facies mosaics and microfacies: an appraisal of some of the key concepts underpinning carbonate sedimentology. *Facies* **51,** 17–23.

Zonneveld, J.P., Gingras, M.K., Beatty, T.W. 2010. Diverse ichnofossil assemblages following the P–T mass extinction, Lower Triassic, Alberta and British Columbia, Canada: Evidence for shallow marine refugia on the northwestern coast of Pangaea. *Palaios* **25,** 368–392.

TABLE AND FIGURE CAPTIONS

Table 1. Facies descriptions and depositional settings.

Figure 1. (a) Geographic location of the French Fork, Beas Lewis Flats and Pleasant Creek sections in the Torrey area (southern Utah). (b) Synthetic lithological succession of the Torrey area and its depositional sequence interpretation.

Figure 2. Field views of the three studied sections and their main lithological units. (a) Lower part of the French Fork section. Note the patchy morphology visible locally in the microbial unit. (b) Beas Lewis Flats section. Note the truncation surface at the top of the microbial limestone unit (white arrows: stratal terminations). (c) Pleasant Creek section. The microbial limestone unit documented both at French Fork and Beas Lewis Flats is absent here.

Figure 3. Legends for French Fork, Beas Lewis Flats and Pleasant Creek log sections.

Figure 4. Log of the French Fork section including lithology, texture and relative abundance of quartz grains. Facies distribution and depositional sequence interpretation is also indicated. See Table 1 for facies descriptions and Figure 3 for legend.

Figure 5. (a) and (b) Field views of the bedding stacking pattern of the microbial limestone unit in the French Fork section. In (a) the black window represents photograph in (c). Some beds show important lateral thickness variations (dashed lines in b) generating dm-patch reef morphologies. (c) and (d) Field view and sketch of a bed that displays a lateral thickness variation in the microbial limestone unit at French Fork. Note that this bed can be subdivided into two subunits: a lower part made of a fenestral limestone subfacies (F3b) and an upper part made of a laminated mudstone subfacies (F3c). (e) Oncoid-ooid-peloidal-intraclast grainstone with fenestrae (F3b). Note the laterally discontinuous stromatolitic crusts that coated some grains (white arrows). (f) Microbial laminae or crusts (F3b; white arrow). (g) Large domal spar-filled sheet cracks (F3c). (h) Mudstone with sparse and laterally discontinuous horizontal cracks, small gastropods and ostracods (F3c).

Figure 6. (a) Field view of a fenestral-rich bed in microbial limestone unit at French Fork. (b) and (c) Thin section and sketch of microbial crusts (both planar and columnar) in a large fenestrae illustrated in (a) (white window). Note that planar stromatolites bind an oolitic grainstone or an oncolitic floatstone and are overlain by columnar stromatolites, which exhibit an upward growth direction inside the fenestrae. (d) Field view of large fenestrae (black arrow) in a bed of the microbial limestone unit at French Fork. (e) Thin section of large fenestrae with downward and upward microbial growth directions (white arrows). (f) and (g) Siliceous sponges in the microbial limestone unit at French Fork section. (f) Sponge in the fenestral limestone subfacies (F3b). The sponge is partially dissolved and replaced by a cavity infilled by microbes and cements. (g) Sponge in the laminated mudstone subfacies (F3c).

Figure 7. (a) and (b) Lateral facies variations observed in a bed of the microbial limestone unit at French Fork. (c) Fenestral limestone subfacies (F3b). Note the internal vadose silts preserved in some fenestrae (white arrow). (d) Laminated facies (F3c) with local small fenestrae and tepee structures (white arrow).

Figure 8. Log of the Beas Lewis Flats section including lithology, texture and relative abundance of quartz grains. Facies distribution and depositional sequence interpretation is also indicated along the section. See Table 1 for facies descriptions and figure 3 for legends.

Figure 9. Field views of (a) a cm-scale domal stromatolite (55.6 m, F2, subunit 1) and (b) subfacies F3a with dense accumulation of gastropods (56.1 m). Beas Lewis Flats section.

Figure 10. Schematic evolution of the main facies types in the microbial limestone unit at Beas Lewis Flats. (a) Synthetic log of the microbial limestone unit (F3) subdivided into 3 subunits. Each bed of the second subunit (see Figs 8, 11) includes a succession of the three subfacies (F3a-c). (b–d) Subfacies F3e, subunit 3. (b) Peloidal, oncoidal, fenestral fabric. (c) Stromatolitic crust showing the alternation of thin dark microbial lamina with ooid-peloidal grainstone. (d) Downward growth of stromatolitic columns with horizontal cracked lamina at the roof of large fenestrae. (e–g) Subfacies F3c, subunit 2. (e) Small columnar to domal stromatolite. (f) Domal muddy sheet cracks. (g) Micrite with gastropods and ostracods. (h–j) Subfacies F3b, subunit 2. (h) Peloid-oncoid-ooid-fenestral grainstone intervals coated with thin microbial lamina. (i) Irregular fenestrae with downward and lateral microbial growth. (j) Subfacies F3c with micrite, ostracods and siliceous sponge (lower-half thin section) and

subfacies F3b with peloidal-fenestral fabric (upper-half thin section). (k–m) Subfacies F3a, subunit 2. (k) Siliceous sponges overlain by gastropod-rich subfacies F3a. (l) Gastropod-rich subfacies F3a directly overlays by planar stromatolites. (m) Intraclastic deposits in subfacies F3a. All thin section illustrations have similar scale bar to (b).

Figure 11. Bed stacking pattern of the microbial limestone unit (subunit 2) at Beas Lewis Flats. (a) Field view of several dm-thick beds displaying similar internal organization. (b) and (c) Field view and schematic sketch of a bed-scale depositional sequence. a.: gastropod-rich basal interval (F3a); b.: fenestral-rich intermediate interval (F3b); c.: Mud sheet crack or stromatolite upper interval (F3c).

Figure 12. Log of the Pleasant Creek section including lithology, texture and relative abundance of quartz grains. Facies distribution and depositional sequence interpretation is also indicated along the section. See Table 1 for facies descriptions and figure 3 for legends.

Figure 13. Field views and thin section illustrations of microbialites observed in the upper Sinbad Formation at Pleasant Creek. (a) Dm-scale domal stromatolites (F4 at around 38.5 m in Fig. 12). (b) Laminated microfabric of stromatolites illustrated in (a). (c) Laminated wavy structures in a dm-thick microbialitic bed (F4 at 45 m in Fig. 14). (d) Laminated microfabric of stromatolites illustrated in (c). (e) Field view of bidirectional cross bedding in oolitic grainstone (F9) in the upper Sinbad Formation. (f) Thin section of oolitic grainstone (F9) with gastropods. (g) Field view and (h) thin section of a peloidal and bioclastic packstone (F13) with bivalves that display umbrella structures with underlying siliceous sponges. Pleasant Creek section.

Figure 14. Depositional models (a) for the red beds of the Black Dragon Formation and microbial limestone unit of lower Sinbad Formation (middle Smithian) and (b) for the bioclastic limestone unit of the upper Sinbad Formation (late middle to late Smithian). See Table 1 for facies description and figure 3 for legends.

Figure 15. Correlation of the French Fork, Beas Lewis Flats and Pleasant Creek sections illustrating the general facies architecture of the Torrey area during the Smithian. S.I to S.V: medium-scale depositional sequences.

Table 1. Facies description and depositional settings.

Facies			Textures	Biotic / non biotic grains	Matrix / cements	Bedding / sedimentary structures	Zones	Environments
F1	Red beds		Dolosiltstones / dolosandstones (conglomerates)	No biota Abundant quartz grains (subrounded to subangular), rare micas and some intraclasts (cm-scale sub-angular to sub-rounded mud chips and mud pebbles). Locally rare primary gypsum needles	Microdolomitic cement	Thin cm-thick (rarely dm-thick) beds. Asymmetrical ripples, climbing ripples, planar et crossed lamination. Tepees, convolutes and very rare and localized bioturbation in the transition beds to F3	Lower intertidal (to shallow subtidal)	Tidal flat
F2	Intraclastic limestones		F	Rare gastropods and siliceous sponge spicules Frequent cm-scale flat pebbles and subangular to subrounded intraclasts, common peloids, rare ooids and oncoids, aggregate grains. Presence of quartz grains and rare micas	Micritic matrix	Thin cm-thick beds with frequent basal erosive surfaces. Presence of tepees, desiccation cracks, fenestrae and few cm-scale stromatolitic domes. Bioturbation. Some crossed lamination and asymmetrical ripples	Subtidal to intertidal	Peritidal / interior platform
F3	Peritidal limestones	F3a - Gastropod-rich	P (G / B)	Abundant gastropods, common ostracods and some siliceous sponges Abundant intraclasts and peloids	Micritic matrix, sparitic cement	Basal bed (cm-thick) intervals, lateraly discontinuous. Basal erosive surfaces. Some fenestrae, micritic geopetal filling of gastropod cavities	Subtidal to intertidal	Peritidal
		F3b - Fenestral	G / P / B	Rare gastropods, ostracods, siliceous sponges and bivalves Abundant oncoids, peloids, aggregate grains. Some ooids and cortoids	Peloidal micrite, sparitic cement	Cm- to dm-thick beds (strong lateral thickness variations). Abundant fenestrae and undulated laminated biofilms	Intertidal	
		F3c - Muddy sheet	M (W / B)	Rare ostracods, small gastropods and siliceous sponges Some intraclasts and mud flakes	Micritic matrix	Dm-thick beds. Laminations with tepee structures and sheet cracks. Some stromatolites, fenestrae and rare bioturbation	Intertidal to supratidal	
		F3d - Oo-pel-oncoidal	G	No biota Abundant peloids, oncoids and ooids	Sparitic cement	Microbial lamination. Some fenestrae	Subtidal gullies	
		F3e - Onco-fenestral	P / G (B)	Common gastropods, some serpulids and ostracods Abundant peloids and oncoids. Some ooids, aggregate grains and mud clasts	Micritic matrix, sparitic cement	Cm- to dm-thick beds. Cm- to dm-longs fenestrae with internal stromatolitic crusts (with upward and downward growth) and stromatactis. Locally, microbial laminated biofilms	Subtidal	
F4	Stromatolitic beds		W / P	No biota Common peloids, some intraclasts	Clotted micritic matrix	Undulated and domal microbial laminations. Tepee structures and fenestrae.	Intertidal (supratidal)	Interior platform (tide dominated)
F5	Dolostones		M / W	Rare bivalves, gastropods and ostracods, often as modic voids. Rare echinoderms Rare to common, locally abundant, quartz grains (sub-rounded to sub-angular). Some intraclasts, mud flakes and peloids. Rare micas	Microdolomitic matrix or cement	Dm- to m-thick intervals of dolostones with cm-thick intercalations of siltstones (more rarely sandstones). Trough cross-stratification, horizontal to low angle planar lamination. Rare bioturbation	Subtidal to intertidal	
F6	Peloidal-intracalstic limestones		P / G	Common bivalves and presence of gastropods Abundant peloids and intraclasts, common cortoids, ooids and aggregate grains. Some oncoids. Rare quartz grains	Peloidal matrix and sparitic cement	Dm- to m-thick beds. Trough cross-stratification and asymmetrical ripples. Some bioturbation	Subtidal to intertidal channels	Tide-dominated shoal complex
F7	Intraclastic rudstone		R	Rare echinoderms (fragments) Common intraclasts (sub-rounded to sub-angular). Some lithoclasts, peloids and ooids	Dolomitized sparitic cement	Cm-thick beds. Asymmetrical ripples and planar horizontal lamniation		
F8	Oo-bioclastic grainstone		G	Common bivalves and gastropods fragments Abundant ooids, some peloids and intraclasts, aggregate grains, oncoids, cortoids and mud flakes. Rare quartz grains	Sparitic cement (micrite matrix)	Dm-thick beds. Asymmetrical ripples and low angle cross-stratification. Rare bioturbation	Subtidal bars	
F9	Pel-bioclastic grainstone		G	Abundant bivalve fragments, some gastropods and rare echinoderms Abundant peloids. Some ooids, oncoids, cortoids and intraclasts	Sparitic cement (micrite matrix)	Cm- to dm-thick beds. Asymmetrical ripples and low angle cross-stratification. Rare bioturbation		
F10	Bioclastic grainstone		G (P)	Abundant bivalves and gastropods. Common echinoderms (fragments) and some serpulids and ammonoids Common peloids and micritic intraclasts. Rare ooids and phosphate grains. Presence of quartz grains	Sparitic to microsparitic cement (peloidal matrix)	Cm- to dm-thick beds. Trough cross-stratification, small asymmetrical ripples. Bioturbation is present		
F11	Bivalve-rich limestones		P / G	Abundant bivalves. Some serpulids, rare gastropods and echinoderms Abundant peloids. Rare intraclasts and phosphate grains. Common sub-rounded quartz grains	Sparitic cement and micritic (peloidal) matrix	Cm- to dm-thick beds. Trough cross-stratification, small asymmetrical ripples. Bioturbation is rare to present		
F12	Bioclastic packstone		P	Abundant bivalves, gastropods and echinoderms. Some ammonoids, serpulids and siliceous sponges Common peloids. Some phosphate grains. Quartz grains are common	Micritic matrix, and locally sparitic cement	Cm-thick beds. Trough cross-stratification, small asymmetrical ripples, horizontal to low angle oblique planar lamination. Common bioturbation	Inner- to mid-shelf transition	Open wave-dominated marine setting
F13	Peloidal-bioclastic limestones		W / P	Common bivalves. Some serpulids, echinoderms, ammonoids, gastropods and siliceous sponges (cf. Dean, 1981) Common peloids, some intraclasts. Common quartz grains, rare micas and very rare detrital dolorhombs	Micritic matrix	Cm-thick beds. Rare trough cross-stratification and asymmetrical ripples. Intense bioturbation	Mid shelf	

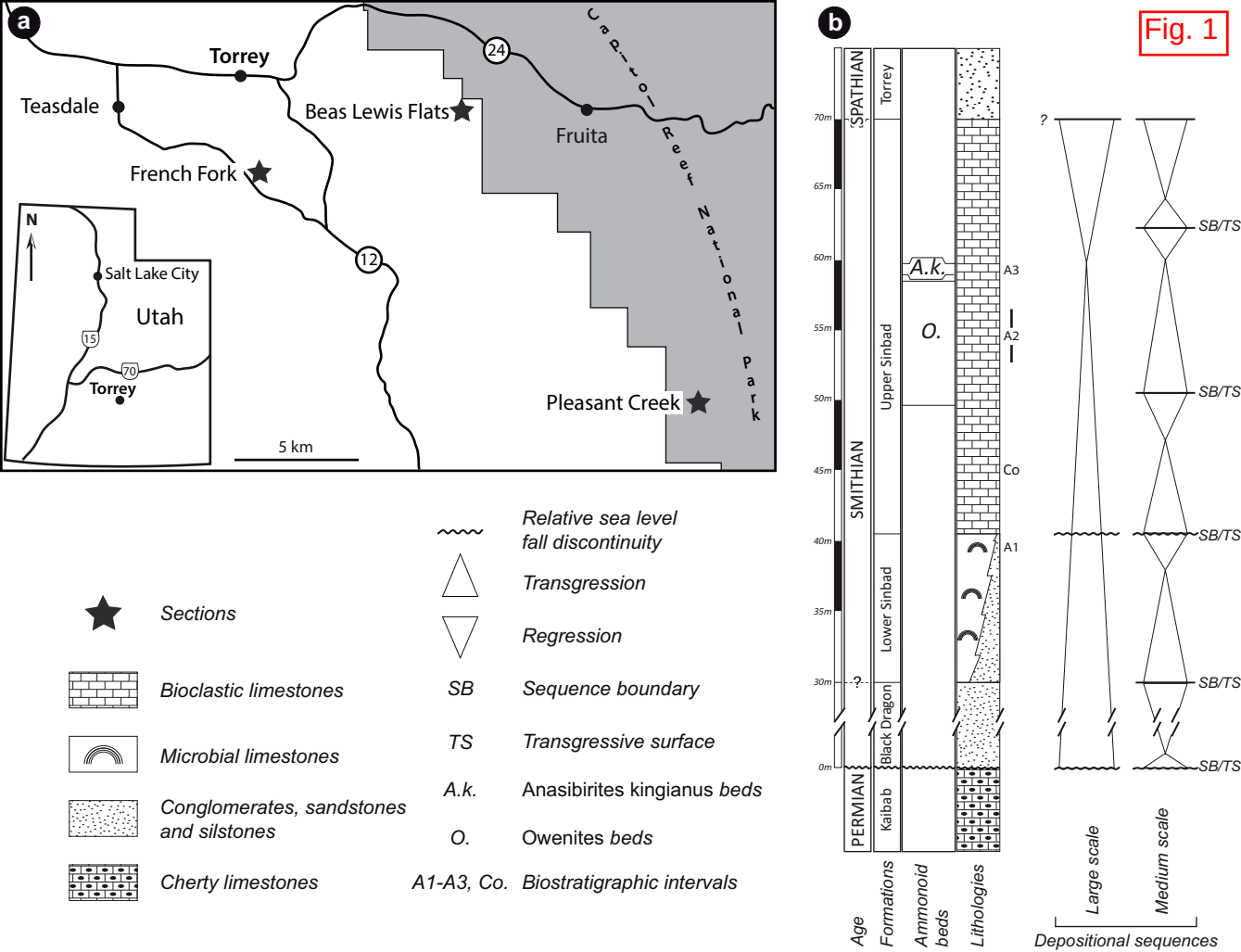
a
Torrey
Teasdale
Beas Lewis Flats
Fruita
French Fork
24
12
Capitol Reef National Park
N
Salt Lake City
Utah
15
70
Torrey
Pleasant Creek
5 km
b
Fig. 1
SPATHIAN
SMITHIAN
PERMIAN
Torrey
Upper Sinbad
Lower Sinbad
Black Dragon
Kaibab
A.k.
O.
A3
A2
Co
A1
70m
65m
60m
55m
50m
45m
40m
35m
30m
0m
?
SB/TS
Sections
Bioclastic limestones
Microbial limestones
Conglomerates, sandstones and silstones
Cherty limestones
Relative sea level fall discontinuity
Transgression
Regression
SB Sequence boundary
TS Transgressive surface
A.k. Anasibirites kingianus beds
O. Owenites beds
A1-A3, Co. Biostratigraphic intervals
Age
Formations
Ammonoid beds
Lithologies
Large scale
Medium scale
Depositional sequences

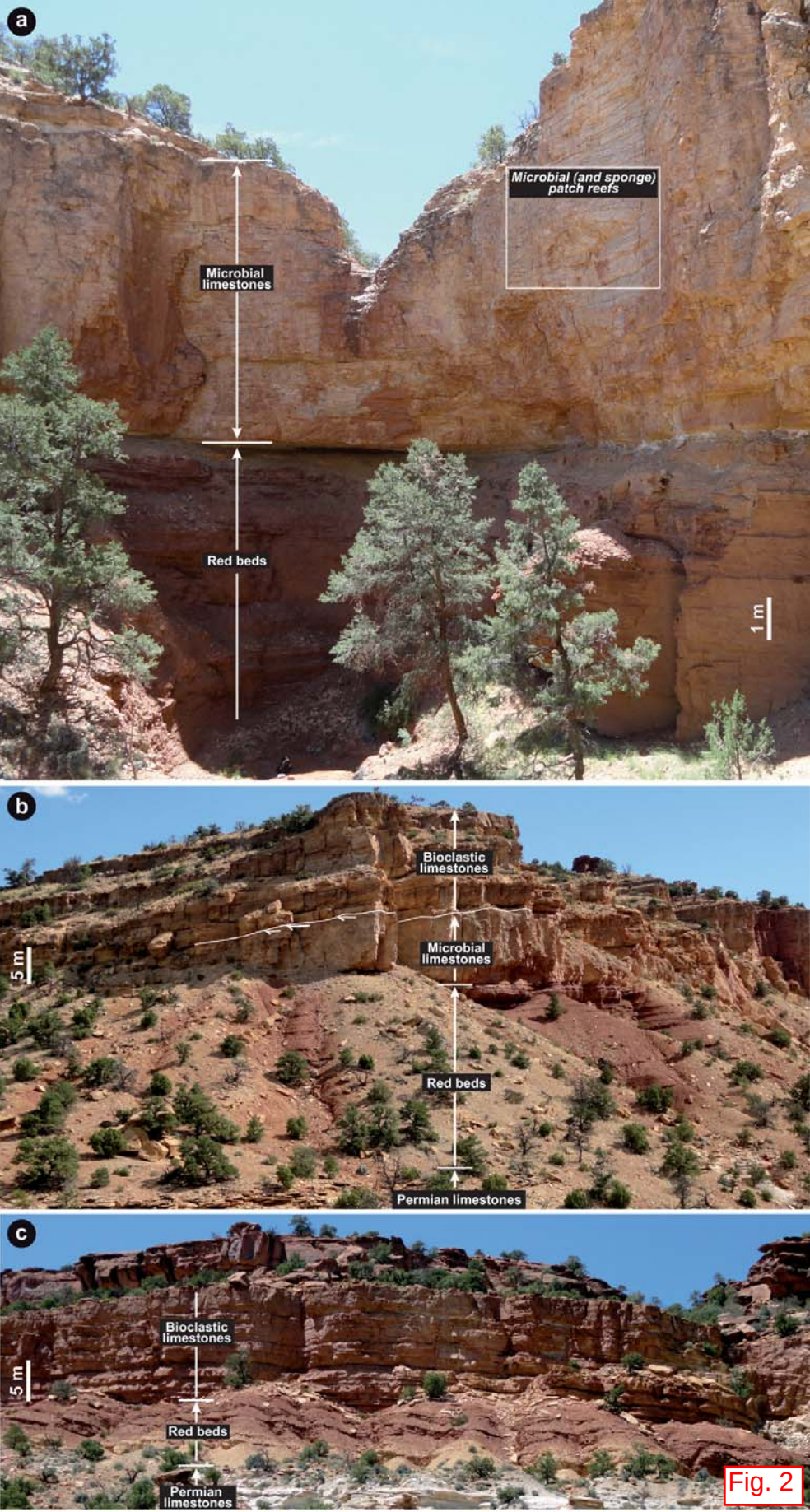
a
Microbial (and sponge) patch reefs
Microbial limestones
Red beds
1 m
b
Bioclastic limestones
Microbial limestones
Red beds
Permian limestones
5 m
c
Bioclastic limestones
Red beds
Permian limestones
5 m

Fig. 2

Fig. 3

Lithologies

- Limestones
- Coarse dolomitic limestones
- Siltstones / sandstones *(s in column textures)*

Biota

- Ammonoids
- Bivalves (undifferentied)
- Echinoderms
- Gastropods
- Ostracods
- Phosphate remains
- Serpulids
- Siliceous sponges
- Sponge spicules

Sedimentary grains

- Peloids
- Coprolites
- Ooids
- Cortoids
- Oncoids
- Aggregates
- Intraclasts
- Flat pebbles
- Mud chips

Textures

- **B** Boundstone
- **G** Grainstone
- **P** Packstone
- **W** Wackestone
- **M** Mudstone

Sedimentary structures

- Bioturbation
- Fluid escapes
- Sheet cracks
- Tepee
- Fenestrae
- Mud cracks
- Cross-bedding
- Planar laminations
- Climbing ripples
- Asymmetric ripples
- Herringbone structures
- Domal stromatolites
- Wavy stromatolites
- Acicular crytals
- Karstification

Microbial structures

- Microbial columns (in large fenestrae)
- Microbial laminae (biofilms)

Quartz abundance

- > 30 %
- 21-30 %
- 10-20 %
- < 10 %

Accommodation

- Decrease
- Increase
- Relative sea-level fall

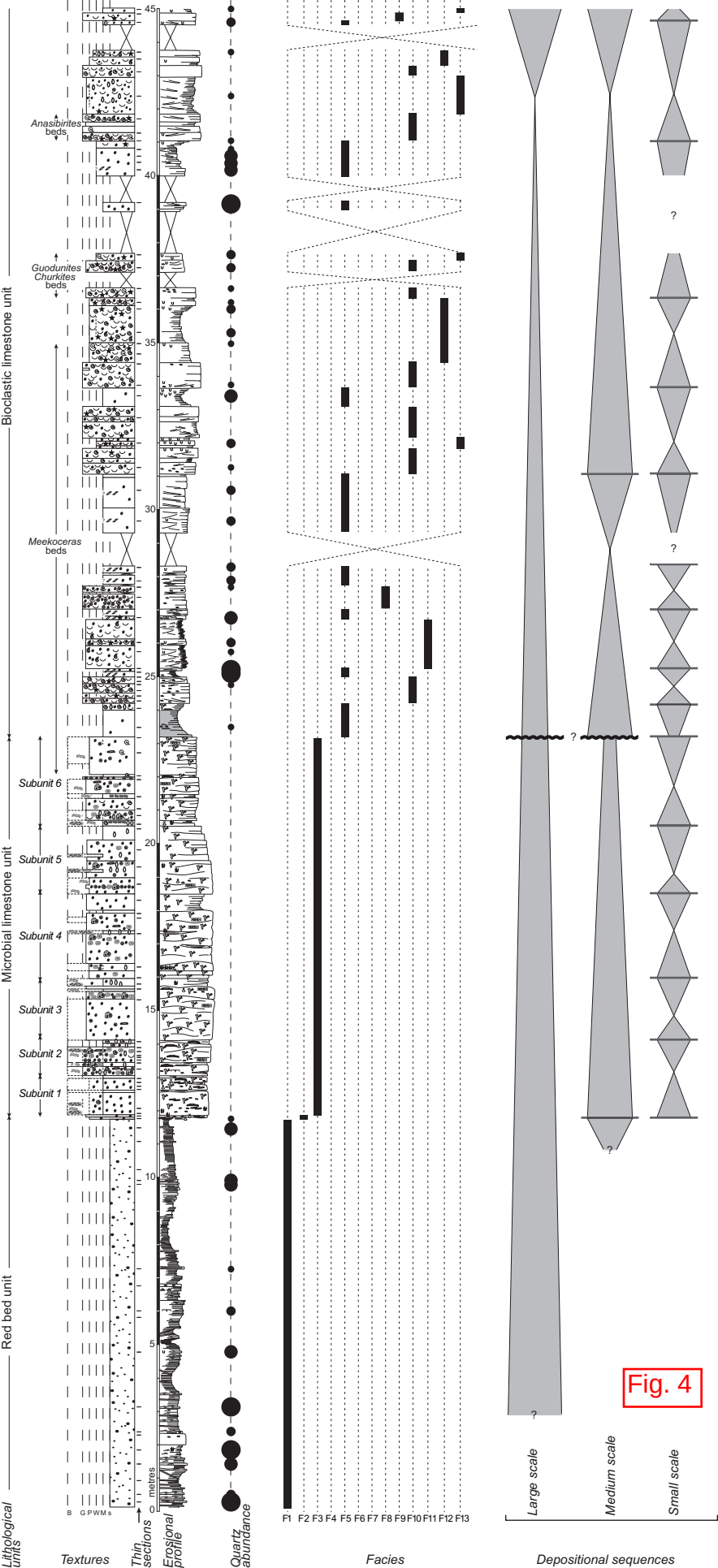
Anasibirites beds
Guodunites Churkites beds
Meekoceras beds
Subunit 6
Subunit 5
Subunit 4
Subunit 3
Subunit 2
Subunit 1
Bioclastic limestone unit
Microbial limestone unit
Red bed unit
Lithological units
metres
B G P W M s
Textures
Thin sections
Erosional profile
Quartz abundance
F1 F2 F3 F4 F5 F6 F7 F8 F9 F10 F11 F12 F13
Facies
Large scale
Medium scale
Small scale
Depositional sequences
Fig. 4

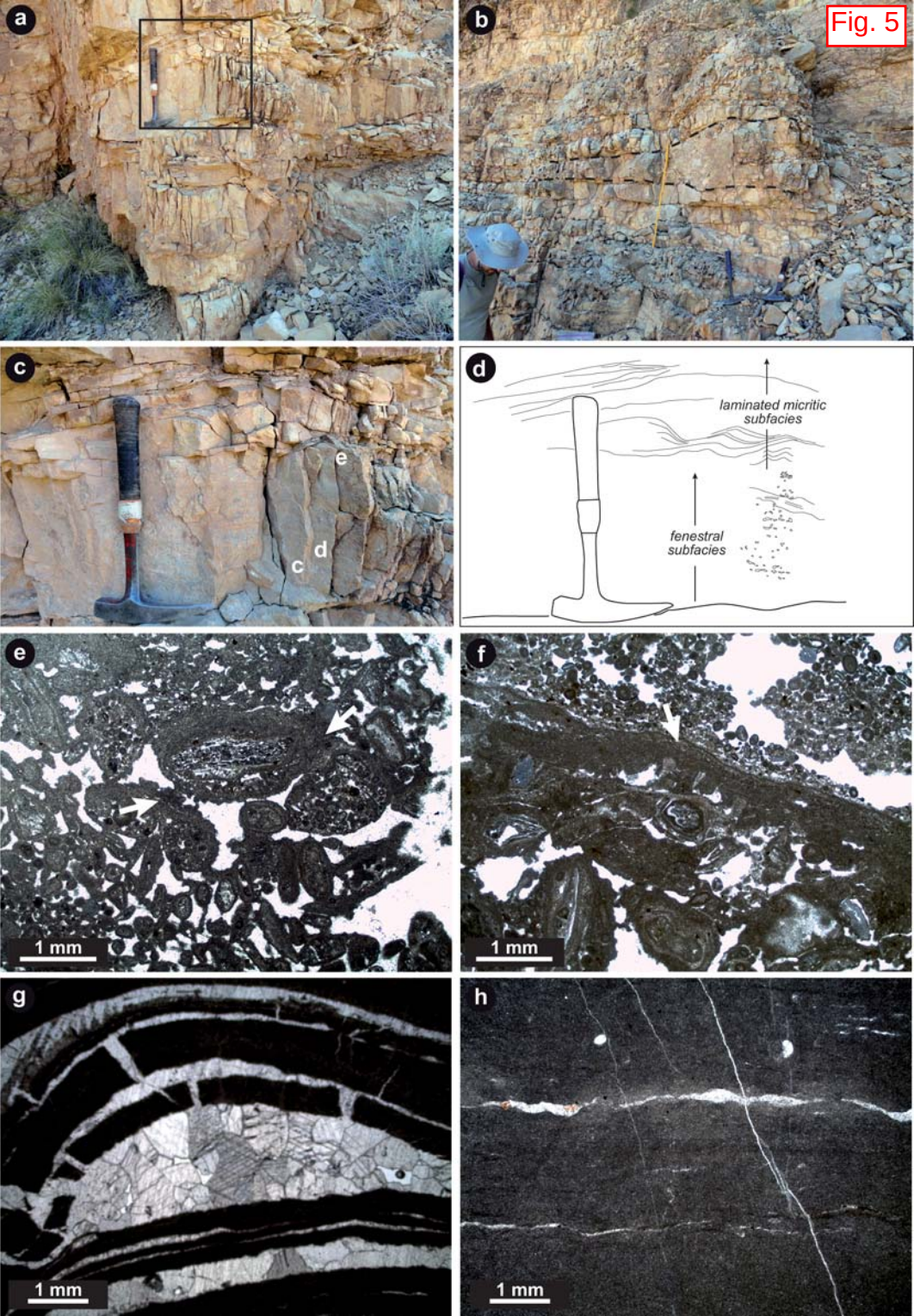
Fig. 5
a
b
c
e
d
c
d
laminated micritic subfacies
fenestral subfacies
e
1 mm
f
1 mm
g
1 mm
h
1 mm

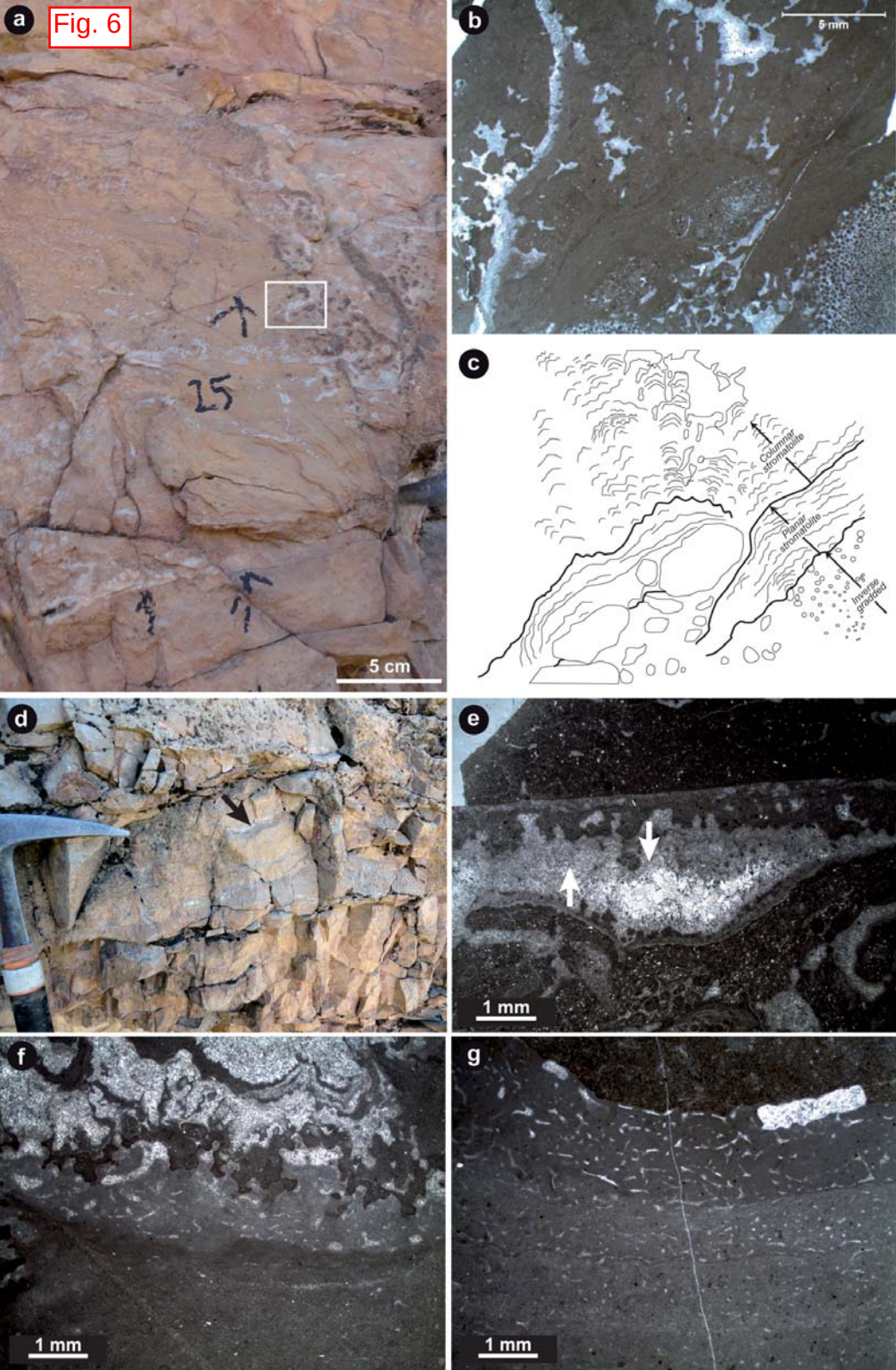
a
Fig. 6
25
5 cm
b
5 mm
c
Columnar stromatolite
Planar stromatolite
Inverse graded
d
e
1 mm
f
1 mm
g
1 mm

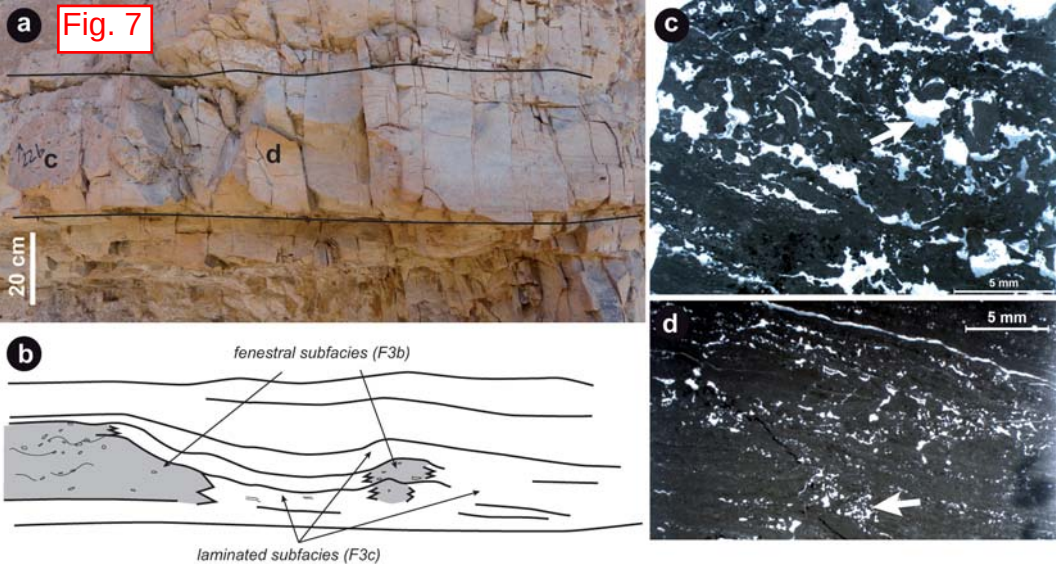
a
Fig. 7
c
d
20 cm
b
fenestral subfacies (F3b)
laminated subfacies (F3c)
c
5 mm
d
5 mm

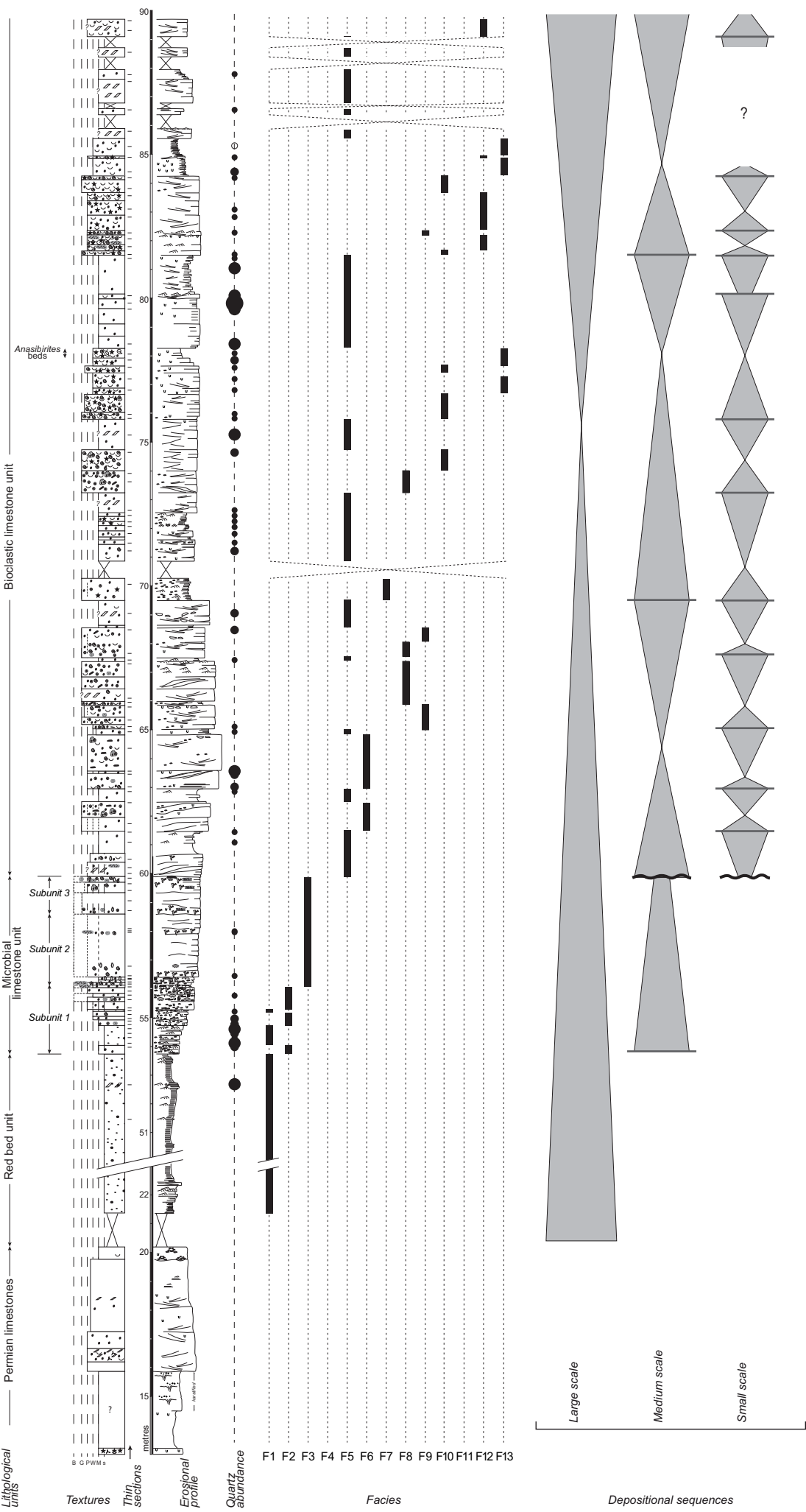
Lithological units
Permian limestones
Red bed unit
Microbial limestone unit
Bioclastic limestone unit
Subunit 3
Subunit 2
Subunit 1
Anasibirites beds
metres
90
85
80
75
70
65
60
55
51
22
20
15
B G P W M s
Textures
Thin sections
Erosional profile
Quartz abundance
F1 F2 F3 F4 F5 F6 F7 F8 F9 F10 F11 F12 F13
Facies
Large scale
Medium scale
Small scale
Depositional sequences

Fig. 8

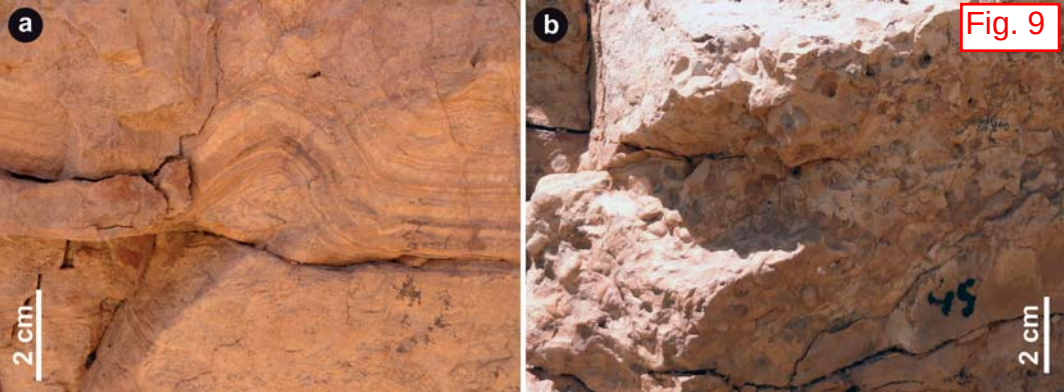
a
2 cm
b
45
2 cm
Fig. 9

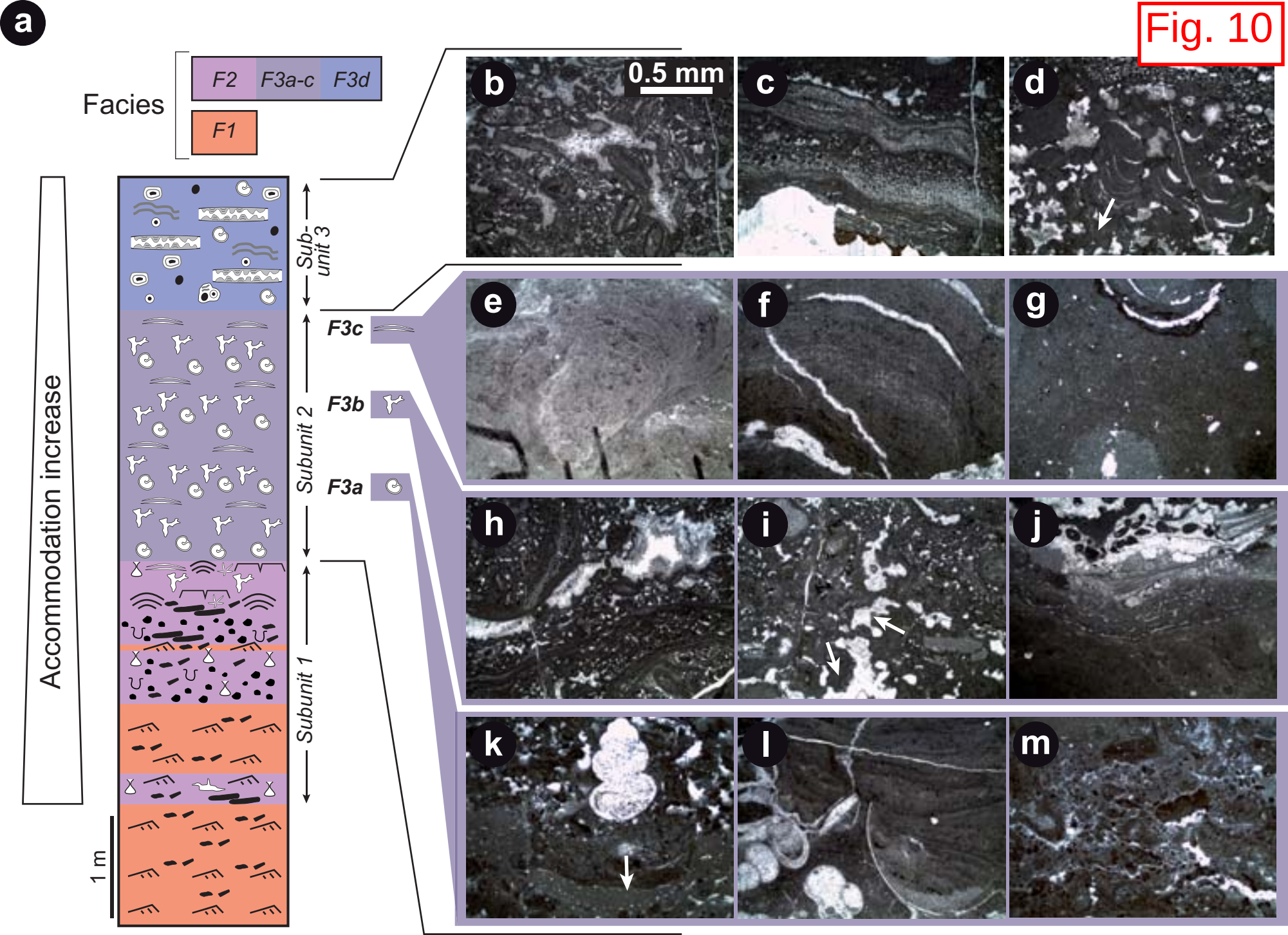
Fig. 10
a
Facies
F2
F3a-c
F3d
F1
Accommodation increase
1 m
Sub-unit 3
Subunit 2
Subunit 1
F3c
F3b
F3a
b
0.5 mm
c
d
e
f
g
h
i
j
k
l
m

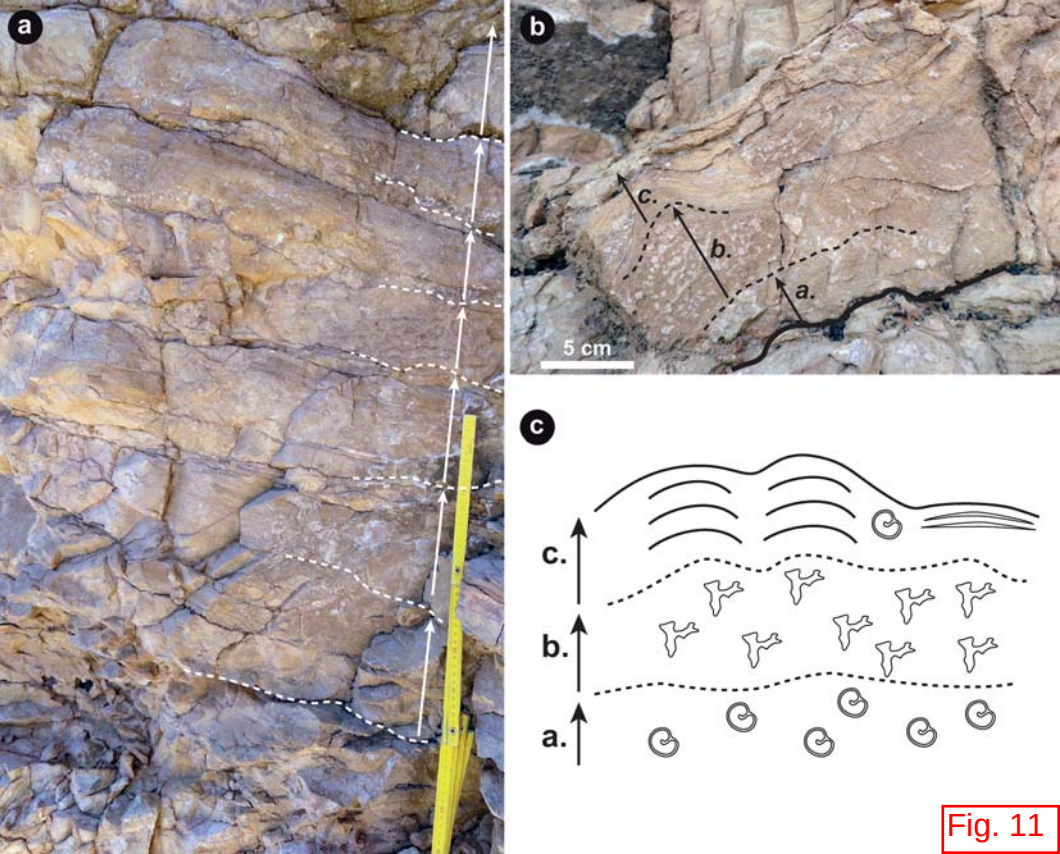

Fig. 11

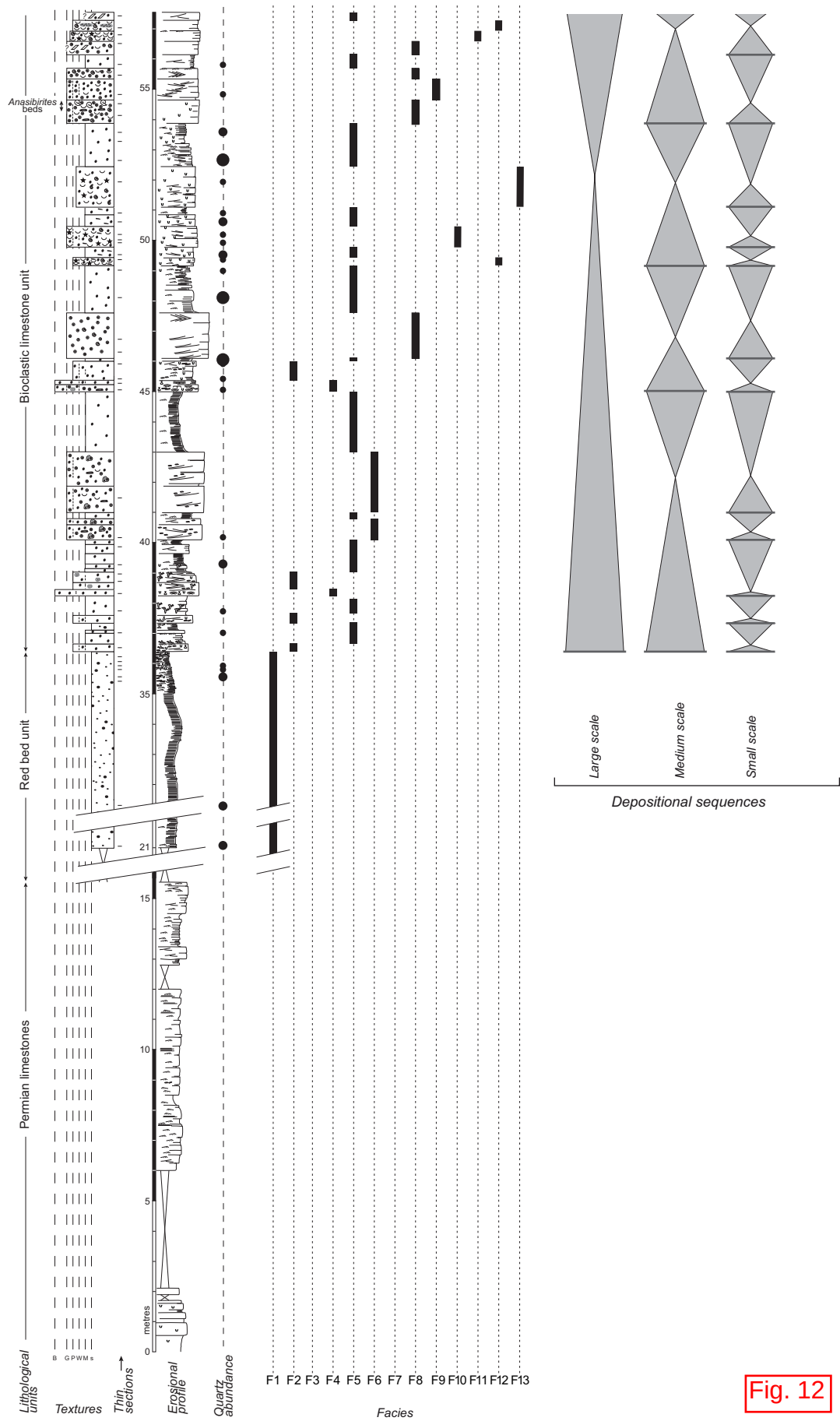
Anasibirites beds
Bioclastic limestone unit
Red bed unit
Permian limestones
Lithological units
Textures
B GPWMs
Thin sections
Erosional profile
Quartz abundance
metres
0
5
10
15
21
35
40
45
50
55
F1 F2 F3 F4 F5 F6 F7 F8 F9 F10 F11 F12 F13
Facies
Large scale
Medium scale
Small scale
Depositional sequences

Fig. 12


a
Fig. 13

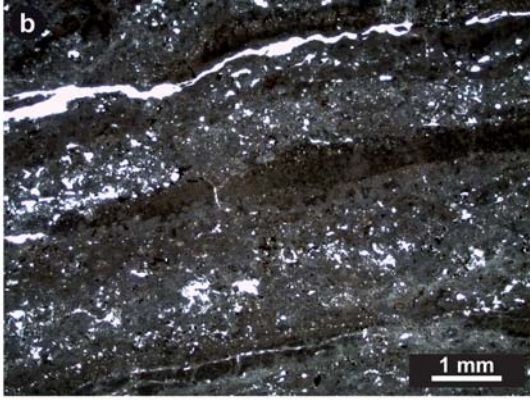
b
1 mm


c

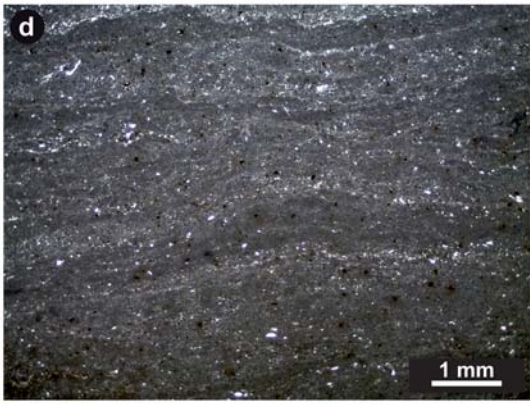
d
1 mm


e

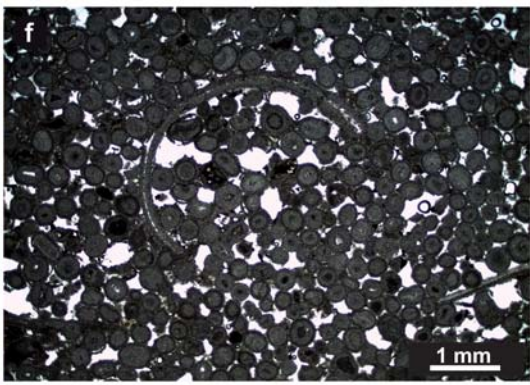
f
1 mm


g


h
1 mm

Fig. 14

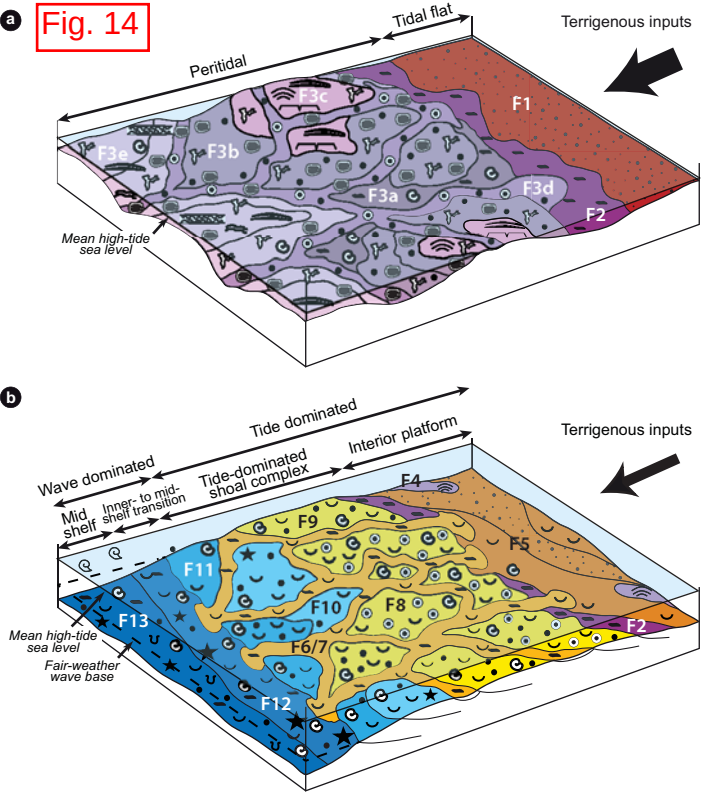

F1: Red beds
F2: Intraclastic limestones
F3: Microbial limestones
F3a: Gastropod-rich
F3b: Fenestral
F3c: Muddy sheet-cracked
F3d: Ooid-peloid-oncoidal
F3e: Oncoid-fenestral
F4: Stromatolitic beds
F5: Dolostones
F6: Peloid-intraclastic limestones
F7: Intraclastic rudstones
F8: Ooid-bioclastic grainstones
F9: Peloid-bioclastic grainstones
F10: Bioclastic grainstones
F11: Bivalve-rich limestones (P/G)
F12: Bioclastic packstones
F13: Peloid-bioclastic limestones (W/P)

N

9 km

FF

BL

16 km

21 km

PC

Beas Lewis Flats

French Fork

Pleasant Creek

TS — *Transgressive surface*

SB — *Sequence boundary*

Medium scale

Small scale

Depositional sequences

Bioclastic limestones
F10-F13

Dolostones F5

Shoal complex
F6-F9

Stromatolites F4

Microbial limestones
F3

Red beds
F1

Permian limestones

Anasibirites beds

S.V

S.IV

S.III

S.II

S.I

TS

SB/TS

unconformity

non-detailed
> 10 m of red beds

non-detailed
30 m of red beds

non-detailed
15 m of red beds

5 metres

Fig. 15